Functional specialization of MITF, TFEB and TFE3 drives radically distinct adaptive gene expression programs in melanoma

Diogo Dias[1], Erica Oliveira[1], Román Martí-Díaz[2], Sarah Andrews[1], Ana Chocarro-Calvo[3], Alice Bellini[1], Laura Mosteo[1], Yurena Vivas García[1], Jagat Chauhan[1], Linxin Li[1], José Manuel García-Martinez[3] José Neptuno Rodriguez-López[2], Silvya Stuchi Maria-Engler[4], Custodia García-Jiménez[3], Luis Sanchez-del-Campo[2], Pakavarin Louphrasitthiphol[1]* and Colin R Goding[1]*

[1] Ludwig Institute for Cancer Research
Nuffield Department of Clinical Medicine
Old Road Campus Research Building
University of Oxford
Old Road Campus
Headington
Oxford
OX3 7DQ
UK

[2] Department of Biochemistry and Molecular Biology A
School of Biology
University of Murcia
Instituto Murciano de Investigación Biosanitaria (IMIB)
30120 Murcia
Spain

[3] Area of Physiology
Department of Basic Health Sciences
Faculty Health Sciences
University Rey Juan Carlos
28922 Alcorcón
Madrid, Spain

[4] Department of Clinical and Toxicological Analysis
School of Pharmaceutical Sciences
University of São Paulo
São Paulo, 05508-000
Brazil.

Running title: MITF family in melanoma

Key Words: MITF, TFEB, TFE3, Melanoma, Melanoma gene regulation

*Corresponding authors:
Pakavarin Louphrasitthiphol
Email: pakavarin.louphrasitthiphol@ludwig.ox.ac.uk
Colin R Goding
Email: colin.goding@ludwig.ox.ac.uk

Lead Author: Colin R Goding; Email: colin.goding@ludwig.ox.ac.uk

Abstract

Within cells multiple related transcription factors targeting the same sequences may co-exist, leading to potential regulatory cooperativity, redundancy or competition. Yet the differential roles and biological functions of co-targeting transcription factors is poorly understood. In melanoma, three highly-related transcription factors are co-expressed: The mTORC1-regulated TFEB and TFE3, that are key effectors of a wide range of metabolic and microenvironmental cues; and MITF, that controls melanoma phenotypic identity. Here we reveal the functional specialization of MITF, TFE3 and TFEB and their impact on cancer progression. Notably, although all bind the same sequences, each regulates radically different and frequently opposing gene expression programs to coordinate differentiation, metabolic reprogramming, protein synthesis, and expression of immune modulators. The results uncover a hierarchical cascade in which microenvironmental stresses, including glucose limitation, lead MITF, TFEB and TFE3 to drive distinct biologically important transcription programs that underpin phenotypic transitions in cancer.

Introduction

Development and homeostasis are underpinned by transcription factors that integrate intra- and extracellular signals to establish and maintain gene expression programs compatible with survival, migration and differentiation. For many cell types, so-called 'master-regulator' transcription factors play a key role in promoting cell identity and differentiation-associated gene expression. Most transcription factors belong to families in which structurally-related DNA binding domains permit recognition of the same or highly-related sequences [1]. Co-expression of more than one family member within a cell can therefore lead to potential regulatory cooperativity, redundancy or competition, and may allow flexibility in controlling common target genes if the co-targeting transcription factors perform non-equivalent functions. However, our understanding of how apparently functionally similar transcription factors may perform distinct roles in the same cell type is limited. This is especially important in cancer where it has emerged that following cancer initiation the subsequent steps in cancer progression are largely driven by microenvironment-mediated changes in cell phenotype [2-4]. For example, as a consequence of nutrient or oxygen limitation encountered as tumors expand, cells employ pro-survival strategies that include modulating their metabolism and adopting an invasive phenotype to escape stress and seek an improved environment [5,6]. Ultimately, whether a cancer cell survives, proliferates or invades may be dictated by the ability of transcription factors to interpret the microenvironment. In this respect, having multiple, highly related transcription factors targeting the same genes but eliciting different outcomes may be a key mechanism that allows cells to undergo appropriate non-genetic adaptations. However, as noted previously [1], understanding synergy, redundancy and the potential for multiple transcription factors able to recognise the same sequence to regulate genes differentially remains a major challenge.

Melanoma represents an excellent model to understand the complex interplay between transcription factors, cell plasticity, the microenvironment and disease progression [7]. Accumulating evidence has implicated the microphthalmia-associated transcription factor MITF, a lineage survival oncogene [8], as a key determinant of phenotypic identity whose expression is suppressed by a range of microenvironmental cues [9] including nutrient limitation [10,11], hypoxia [12,13] and inflammatory signaling [10]. Importantly, MITF plays a critical coordinating role in many aspects of melanoma cell biology by promoting survival [8,14], proliferation [15,16] and differentiation [17,18], regulating metabolism [13,19-21], controlling DNA damage repair [22,23], and suppressing senescence [24] and invasion [25]. Significantly, MITF levels in vivo are dynamic [26], and MITF expression is suppressed in invasive cells [25] that have elevated tumor-initiating ability [10,27] and exhibit non-genetic therapy resistance [28-31]. However, for invasive cells to generate a new metastasis, MITF should be re-expressed to allow proliferation [18,32].

Since metastasizing and tumor-initiating cells are predominantly $MITF^{Low}$, it seems likely that microenvironmental cues that downregulate MITF will also upregulate pro-survival mechanisms that facilitate metastatic dissemination, but which may also slow proliferation. Yet the molecular adaptations

that take place as cells are subject to potentially lethal stresses during disease progression remain poorly understood.

One intriguing possibility yet to be fully explored is that on downregulation of MITF, the MITF-related transcription factors TFEB and TFE3 [9,33,34] take on MITF functions. TFE3 and/or TFEB are key regulators of autophagy and lysosome biogenesis [33,35-37], but also have been implicated in a wide range of other critical cellular processes in many tissue types. For example, in modulating the integrated stress response [38,39], insulin expression [40], the innate immune response [41,42], recovery from exercise [43] and lineage specification and stem cell fate [44,45]. Unlike the melanocyte/melanoma-specific isoform of MITF (MITF-M), TFE3 and TFEB are regulated primarily by nuclear/cytoplasmic shuttling. In nutrient rich conditions TFEB and TFE3 are retained in the cytoplasm via 14-3-3 protein interaction [46] following their phosphorylation by the Mammalian Target of Rapamycin Complex 1 (mTORC1) complex [33,47]. mTORC1-mediated phosphorylation of TFEB and TFE3 requires their recruitment to endolysosomal membranes by the RAGC/D GTPases [48] where their phosphorylation is dependent on Folliculin (FLCN), a RAGC-activator [49]. An additional RAG-dependent phosphorylation event leads, under nutrient replete conditions, to $CUL^{\beta-TrCP}$-dependent ubiquitination and degradation of TFE3 and a non-melanocyte MITF isoform, MITF-A, but not TFEB [50]. On nutrient limitation, decreased mTORC1 activity and dephosphorylation by calcineurin [51] and/or PP2A [52] lead TFEB and TFE3 to translocate to the nucleus to regulate their target genes. In most studies, TFEB and TFE3 regulate the same genes in a similar way. However, whether they control an identical gene expression program in all cells has not been explored in detail, and it remains a possibility that each factor may regulate both common and unique gene sets. Not surprisingly, given their physiological importance, deregulation of TFEB and TFE3 activity is increasingly recognized as contributing to cancer [53-56].

Here we investigate the potential role of TFEB and TFE3 in cells that also express MITF to understand better the potential of these transcription factors to exhibit distinct and non-redundant roles in melanoma progression. Strikingly, we find that while all members of the MITF family exhibit a similar genome-wide occupancy, their ability to regulate gene expression alone or in combination is radically different.

Results

MITF controls mTORC1 signaling

Previous work in melanoma has shown that invasion, and an $MITF^{Low}$ state, can be mediated as a consequence of nutrient limitation [5,10,11]. Yet if starvation can trigger invasion, why would $MITF^{Low}$ cells maintain an invasive phenotype under nutrient-rich culture conditions? We hypothesised that loss of MITF expression might lead to a failure to sense or use nutrients so that cells would maintain an undifferentiated state even under nutrient replete conditions. Many microenvironmental triggers that promote invasion and downregulate MITF, such as low glucose or amino acid levels, also decrease signalling through mTORC1, that promotes protein translation when amino acids are abundant, by promoting S6 kinase-mediated

activation of S6, and phosphorylation of 4EBP1 [57]. Therefore, as a first step to investigating any potential failure to sense nutrients in MITF^{Low} melanoma cells, we examined the effect of MITF depletion on mTORC1 activity. Depletion of MITF using siRNA in two MITF^{High} cell lines (IGR37 and HBL) led to a reduction in S6 phosphorylation, and reduced 4EBP1 phosphorylation, marked by a switch from the upper to lower band (**Figure 1A**), indicating a reduction in canonical mTORC1 signaling. This observation is consistent with MITF^{Low} cells being slow-cycling [25,27]. The decreased mTORC1 activity arising as a consequence of MITF depletion could be accounted for, at least in part, by the concomitant increase in expression of PTEN, an inhibitor of PI3 kinase that lies upstream from mTORC1.

To identify potential PTEN-independent mTORC1 inhibitory mechanisms that might be activated as MITF^{High} melanoma cells transition to an MITF^{Low} state, we next examined expression of two alternative regulators of mTORC1 activity: the RAG GTPase and the folliculin-interacting protein 2 (FNIP2), that together modulate mTORC1 signaling at the lysosome [49,58-60] and consequently control the activity of the MITF-related factors TFEB and TFE3. In the Cancer Cell Line Encyclopedia (CCLE) expression of *RRAGD*, but not other RRAG genes, as well as *FNIP2,* exhibit close correlation to expression of MITF (**Figure 1B)**. The correlation between *RRAGD* and *FNIP2* expression with that of *MITF* was reproduced in an independent dataset from Tsoi et al [61] in which 53 melanoma cell lines established from patient biopsies were clustered into 4 distinct phenotypes (**Figure 1C)**. In these melanoma cells *RRAGD* and *FNIP2* mRNA levels were strongly expressed in the MITF^{High} transitory and melanocytic phenotypes and not in the undifferentiated or neural crest-like phenotypes. The correlation between *RRAGD* and *FNIP2* mRNA expression and that of MITF was also found in The Cancer Genome Atlas (TCGA) melanoma cohort (**Figure 1D**). Importantly, examination of a previously published [62] ChIP-seq dataset revealed binding by MITF to the promoters of the *RRAGD* and *FNIP2* genes (**Figure 1E),** and expression of *FNIP2*, and especially *RRAGD,* were both lower in the WM793 and IGR39 MITF^{Low} melanoma cell lines compared to MITF^{High} IGR37 and 501mel cells (**Figure 1F)**. Doxycycline-mediated induction of β-catenin (CTNNB1), an MITF co-factor [63] and activator of MITF expression [64], in the MITF^{High} IGR37 melanoma cell line increased *FNIP2* and *RRAGD* expression 4.5 and 9.3-fold respectively (**Figure 1G)**, while depletion of MITF using shRNA decreased *RRAGD* and *FNIP2* mRNA expression (**Figure 1H)**. Collectively these data strongly suggest that *FNIP2* and *RRAGD* are direct MITF target genes.

Collectively these observations suggest that in MITF^{Low} melanoma cells where mTORC1 signaling is low and *RRAGD* and *FNIP2* expression is reduced, TFEB and TFE3 would potentially be active. However, given that the historic focus on MITF, the role and regulation of TFEB and TFE3 in melanoma has been largely neglected, and their impact on melanoma progression remains poorly understood compared to that of MITF.

Differential regulation of TFEB and TFE3 in melanoma by glucose limitation

To understand the potential role of the MITF-related transcription factors TFEB and TFE3 in melanoma, especially as melanoma cells transition from an MITF^{High} to an MITF^{Low} state, we first analysed their

expression relative to MITF. In the TCGA melanoma cohort ranked by *MITF* expression, *TFE3* mRNA exhibited an inverse correlation with that of MITF (**Figure 2A**). *MITF* mRNA levels also showed a moderate anti-correlation with that of *TFEB* (**Figure 2B**) while *TFEB* and *TFE3* mRNA exhibited a good correlation (**Figure 2C**). These observations are consistent with previous examination of *TFEB*, *TFE3* and *MITF* mRNA expression in melanomas [65]. However, since TCGA melanomas contain multiple non-melanoma cell types including infiltrating immune cells and fibroblasts, we also examined the relative expression of *TFEB* and *TFE3* mRNA in the Tsoi et al [61] panel of 53 melanoma cell lines grouped according the phenotype (**Figure 2D**). These results again showed that *TFE3* mRNA was predominantly expressed in the $MITF^{Low}$ undifferentiated and neural crest-like phenotypes, rather than the $MITF^{High}$ transitory and melanocytic phenotypes. By contrast, *TFEB* mRNA expression was not restricted to any phenotype. In an additional in-house panel of 12 cell lines grouped by *MITF* expression, mRNA-seq again indicated predominantly low *TFE3* expression in $MITF^{High}$ cell lines while *TFEB* mRNA expression was relatively variable (**Figure 2E**). Since TFEB and TFE3 are primarily regulated post-translationally though nuclear/cytoplasmic shuttling, we also examined their protein expression. The results (**Figure 2F**) indicated that TFEB protein was more expressed in cell lines expressing MITF, with SKmel28 a notable exception, but TFE3 was expressed largely independent of MITF status. Thus, in some cells TFE3 is the only MITF family member expressed.

Immunofluorescence using two $MITF^{High}$ (501mel and IGR37) and two $MITF^{Low}$ (IGR39 and WM793) cell lines revealed a low expression of TFEB that was largely nuclear (**Supplemental Figure 1A**). This was surprising given that TFEB in many cell lines has been reported to be predominantly cytoplasmic under nutrient replete conditions. Nevertheless, treatment with Torin, a specific inhibitor of mTOR, substantially increased the levels of nuclear TFEB in all cell lines, indicating that TFEB is regulated by mTOR activity, though the increase was less apparent in the $MITF^{Low}$ cells. Using anti-TFE3 we again observed largely nuclear staining in the $MITF^{High}$ 501mel and IGR37 cells lines with the level of nuclear TFE3 being increased by Torin. However, in IGR39 cells, unlike TFEB, TFE3 was predominantly cytoplasmic but was nuclear following Torin treatment. In WM793 cells only very low levels of cytoplasmic TFE3 were observed, with Torin inducing a moderate shift to the nucleus.

That TFEB is phosphorylated by mTOR was confirmed by Western blotting for fractionated extracts from 501mel cells transfected with control or MITF-specific siRNA (**Supplemental Figure S1B**). In this cell line whole cell extracts revealed that Torin induced a loss of the slow migrating phosphorylated form of TFEB and accumulation of nuclear TFEB. On depletion of MITF there was a similar accumulation of nuclear TFEB using Torin, but the levels of cytoplasmic phosphorylated TFEB were reduced. Notably, tissue sections from three different human melanomas using immunocytochemistry revealed a significant proportion of melanoma cells exhibiting strong nuclear staining of TFEB (**Supplemental Figure S1C**), consistent with other work that revealed 63% of melanoma metastases exhibit nuclear TFE3 staining [66].

Although it is widely assumed that TFEB and TFE3 are regulated in a very similar way, our observations regarding their expression in melanoma led us to examine whether specific microenvironmental stresses

might differentially control TFEB and TFE3. In particular, we were interested in glucose limitation, frequently found in tumors, that we showed previously can regulate TFEB nuclear/cytoplasmic shuttling [67]. Consistent with our previous observations, upon glucose starvation, conditions under which MITF is silenced over time (**Figure 2G**) [11], TFEB initially exhibited at 4 h a faster mobility characteristic of its nuclear accumulation [49,67,68]. However, by 24 h TFEB expression was strongly repressed (**Figure 2G**). By contrast, expression of TFE3 was not silenced, even after 48 h glucose deprivation by which time it was the only MITF-family member expressed. The differential regulation by low glucose of MITF and TFEB versus TFE3 is not restricted to melanoma as similar results were also found in HT29 colon cancer cells (**Figure 2H**); after initially exhibiting a faster migration following glucose removal, TFEB is largely repressed by 24 h, whereas by contrast TFE3 is up-regulated. Collectively these results suggest that under conditions such as glucose limitation where cells transition from an $MITF^{High}$ to $MITF^{Low}$ state, TFEB is initially activated but its expression is ultimately lost and TFE3 becomes the predominant MITF family member expressed. Since low glucose drives a switch away from MITF and TFEB to a TFE3-only state we asked whether depletion of TFE3 might affect the cell cycle or survival in glucose deprived cells. We therefore transfected IGR37 melanoma cells using a pool of TFE3-specific siRNAs for 48 h before placing cells in glucose free medium. The results **(Figure 2I)** revealed that in low glucose, depletion of TFE3 led to a dramatic increase in the sub-G1 population and corresponding decrease in G1 cells, suggesting that TFE3 plays a key pro-survival role under these conditions.

Collectively these observations prompted us to examine the potential differential regulatory role of MITF, TFEB and TFE3 n melanoma.

MITF, TFE3 and TFEB bind a similar repertoire of genes

Under some conditions MITF, TFEB and TFE3 may be differentially expressed. For example, under long-term glucose limitation, expression of MITF and TFEB is suppressed, but TFE3 expression is maintained. However, whether all three factors can bind and regulate the same genes in the same cells is unknown. Although all three proteins have an identical basic region that makes sequence specific DNA contacts (**Figure 3A**), it is possible that differential interaction with cofactors might enable to them to either bind or differentially regulate specific subsets of genes. As a first step to investigating this possibility we generated 501mel human melanoma cells in which HA-tagged TFEB and TFE3 were expressed under the control of a doxycycline (Dox)-inducible promoter and performed ChIP-seq using the HA antibody. $MITF^{High}$ 501mel cells were used since we have used a similar approach in this cell line to map successfully the genome-wide binding of MITF [62,69] with the use of the anti-HA antibody providing increased immunoprecipitation efficiency and specificity.

Western blotting of 501mel cells expressing HA-TFEB revealed that doxycycline was able to induce TFEB expression (**Figure 3B**). Since TFEB is inhibited by mTORC1 we performed ChIP-seq using either 0 ng or 5 ng of Dox with or without treatment with 250 nM Torin that could induce the nuclear accumulation of the HA-tagged TFEB (**Supplemental Figure S2A**). ChIPs were performed in duplicate and peaks

assigned if they were at least 4-fold above the input control with replicates showing a good concordance (**Supplemental Figure S2B).** The results (**Figure 3C**) revealed substantial genome occupancy even in the absence of both Dox and Torin, indicating that even when expressed at a low level in the absence of Dox, TFEB expression was able to enter the nucleus and bind DNA, consistent with previous work indicating that TFEB cycles in and out of the nucleus even under nutrient rich conditions [67,70]. Treatment with Torin increased the numbers of binding sites recognised (**Supplemental Figure S2C)** with an additional 4906 sites recognised compared to 3490 bound in common between untreated cells or those exposed to Torin. Although, there was no significant difference in the mean peak score, the median was lower under Torin treatment alone. This was due to the average peak score being reduced by the additional and weaker binding sites which were only detectable following Torin treatment. In the presence of 5 ng Dox, HA-TFEB expression was increased to levels similar to that of the endogenous protein, and TFEB binding was also increased compared to the no-Dox condition with 9576 sites occupied (**Supplemental Figure S2D),** versus 4005 (**Supplemental Figure S2C)**. This is consistent with previous work with MITF that showed increased expression leads to recognition of more sites genome wide with increased occupancy at any individual site [62,69]. Using a combination of Dox and Torin led to a total of 39,582 sites being occupied (**Supplemental Figure S1D)** of which 9522 were bound in common to the Dox-only condition and an increased mean peak score (**Figure 3C**). These data were reflected in the read density maps (**Supplemental Figure S2E).**

We next repeated the ChIP-seq using HA-TFE3 in the absence of Dox to maintain a level of TFE3 similar that in parental cells (**Figure 3D**). Torin again promoted the nuclear localization of HA-TFE3 (**Supplemental Figure S2F)** with good concordance between the replicates (**Supplemental Figure S2G, H).** When comparing the overlap between the binding of TFE3 with that of TFEB in the absence of doxycycline but in the presence of Torin, the results (**Figure 3E**) revealed 37,626 peaks bound by both factors. 1956 TFEB peaks and 44,970 TFE3 peaks were unique. A 3-way comparison with the previously published [62] MITF ChIP (**Figure 3F**) revealed 37,123 sites bound by all three factors, but also a large number of peaks bound by each factor alone or by any two factors. For example, MITF and TFE3 share 32,649 binding sites that are not bound by TFEB. The number of binding sites for each factor will depend in part on relative expression levels, post-translational modifications, and immunoprecipitation efficiency. We hypothesised that the majority of sites not bound by all three factors might be relatively low affinity sites that would be reflected in a lower peak score. We therefore quantified the peak score of binding sites for each combination of factor (**Figure 3G**). As anticipated, the peak score of those sites bound by all three factors was higher than those bound by any other single or combination of factors, with the lowest peak score associated with the unique MITF peaks. Taken together, our interpretation of these data is that high peak score reflects sites with a higher affinity, and that higher affinity will be more likely to lead to productive gene regulation than those sites with a very low affinity/peak score. Overall, while we cannot rule out binding by individual factors to unique genes, it seems likely that the vast majority of potential regulatory sites are bound by all three factors. Moreover, motif analysis revealed that all three MITF family members recognised a similar 8 bp consensus TCACGTGA (**Figure 3H)**, as previously identified for MITF

[71], also known as the CLEAR box [35]. In line with a common target sequence, all three factors also exhibited a similar genomic distribution with the majority of binding in intergenic regions and introns (**Figure 3I)**. Consistent with all three proteins binding similarly regulated genes, all showed binding to the promoters of known MITF targets, *TYR* and *MLANA*, implicated in melanocyte differentiation and melanin production, as well as *CDK4* and the fatty acid desaturase *SCD* (**Figure 3J)**.

MITF family members regulate different gene sets

The results so far indicate that as expected, given their highly similar DNA-binding domains, MITF, TFEB, and TFE3 bind a similar repertoire of genes. However, DNA binding determined by ChIP-seq does not necessarily equate to regulation of the corresponding genes [72]. Moreover, while TFEB and TFE3 are both inhibited by mTORC1 signaling and are widely assumed to perform similar functions, it remained a possibility that they do not perform an equivalent role on all genes. We therefore examined the contribution of each factor to gene expression.

We initially used $MITF^{High}$ 501mel human melanoma cells that express all three factors (**Figure 2F**). Since TFE3 and TFEB are activated by amino acid limitation that decreases mTORC1 signaling, we first performed RNA-seq in triplicate on 501mel cells exposed to HBSS that contains glucose but lacks amino acids. The results revealed over 2400 differentially expressed genes DEGs (FC $\geq$ 2, p <0.05) (**Figure 4A**) with 1254 genes significantly down-regulated and 1167 up-regulated (**Figure 4B, Supplemental Table S1**). Consistent with lack of amino acids driving a cell cycle arrest, Gene Set Enrichment Analysis (GSEA) (**Figure 4C, D**) revealed major down-regulation of the HALLMARK E2F1 and MYC TARGET gene sets as well as genes associated with DNA repair that have previously been reported to be targets of MITF [22,24,73,74].

To determine the repertoire of genes regulated by MITF, TFEB and TFE3 in these cells we next used CRISPR/Cas9 to knockout (KO) each gene. While we were successful in inactivating *TFEB* and *TFE3*, and also in making a *TFE3/TFEB* double knock-out (DKO) (**Figure 4E**), we were unable to generate an *MITF* KO, likely because the *MITF* gene in these cells is present in multiple copies. Of the two *TFEB* KO cell lines generated both exhibited a moderate up-regulation of the TFE3 protein, but had no effect on MITF expression. The *TFE3* KO cells exhibited some downregulation of TFEB, more so in clone 2, and also a moderate suppression of MITF expression. Triplicate RNA-seq analysis of a *TFEB* (Clone 2) and *TFE3* (Clone 1) KO, and the DKO grown under standard culture conditions revealed both upregulation and downregulation of genes (**Figure 4F,G**), consistent with TFEB and TFE3 possessing transcriptional activity even under nutrient replete conditions. Importantly, GSEA (**Figure 4H**) revealed that KO of *TFE3* or *TFEB* had fundamentally different effects on gene expression. When comparing the *TFE3* KO to the parental 501mel cells, we noted significant (adjusted *p-value* < 0.05) enrichment of the E2F TARGETS and G2M CHECKPOINT gene sets, and downregulation of gene sets including HYPOXIA, COMPLEMENT, IL2/STAT SIGNALING and APOPTOSIS (**Figure 4H**, highlighted in green). By contrast, in the *TFEB* KO compared to the parental cells, each of these gene sets were regulated in the opposite way. In addition,

the Epithelial Mesenchymal Transition (EMT) gene set was strongly upregulated in the *TFEB* KO, but not in the *TFE3* KO, while MTORC1 SIGNALING was down-regulated in the *TFE3* KO and the *TFE3/TFEB* DKO, but not the *TFEB* KO. Many of the gene sets that displayed significantly different expression in the single KOs were not differentially expressed in the DKO, suggesting that the effect of one KO was at least partly reversed by the KO of the related gene.

Blockade of mTOR using Torin, a selective mTOR inhibitor, can induce nuclear accumulation of TFEB and TFE3 and consequently enhance their ability to regulate gene expression. We therefore assessed the effect of *TFE3* and *TFEB* KO in the presence or absence of Torin. As expected, Torin treatment of the parental cells or the *TFE3* KO, the *TFEB* KO or the DKO led to both upregulation and downregulation of gene expression (**Supplemental Figure S3A, B**). We next used GSEA to identify gene sets significantly (adjusted p-value <0.05) differentially regulated under Torin treatment. Consistent with Torin blocking mTORC1 signaling, in the parental cells we observed significant downregulation of the mTORC1 signaling gene set, as well as the MYC and E2F TARGET gene sets (**Supplemental Figure S3C,** top left), as was also observed using HBSS (**Figure 4C**). Also noted was upregulation of the EMT gene set on Torin treatment.

We next compared the effect of Torin on the *TFE3* KO cells to that of Torin on parental cells (**Supplemental Figure S3D**). Remarkably all differentially expressed gene sets were downregulated and none were significantly upregulated. The *TFE3* KO therefore appears to amplify the effect of Torin, leading to strong suppression of gene sets associated with mTORC1 SIGNALING, CHOLESTEROL HOMEOSTASIS, as well as E2F and MYC TARGETS. Notably the upregulation of the EMT gene set in parental cells exposed to Torin was reversed in the Torin-treated *TFE3* KO.

When comparing the effect of Torin on the *TFEB* KO cells to that of Torin on parental cells (**Supplemental Figure S3E**), we again obtained a result largely the opposite to that seen using the *TFE3* KO, and for some gene sets the effect of Torin on parental cells was reversed. For example, the expression of the MTORC1 SIGNALING gene set was reduced in both the parental and *TFE3* KO cells on Torin treatment, but was increased in the *TFEB* KO cell line. By contrast the MYC TARGETS V1 gene set was decreased in the parental and both *TFE3* and *TFEB* KO cell lines on Torin treatment, as well as in the DKO (**Supplemental Figure S3F**).

Collectively these data indicate that while both TFE3 and TFEB activity are controlled by nutrient availability, and both bind a similar repertoire of target genes, surprisingly their global effects on gene expression may be very different. However, the interpretation of the data is complicated by the fact that we were unable to KO MITF in the 501mel cells used for these analyses. It is possible that high levels of MITF might compete with binding of TFE3 or TFEB on some genes, or might mask the effects on gene expression of the KO of either. We therefore chose to complement the analysis in 501mel cells by using a previously described [75] murine B16/F10 cell line in which *MITF* had been knocked-out to reveal a role for MITF in suppression of NK-cell mediated killing (**Figure 5A)**. Note that on close inspection of this Western blot there is a low level of a fast-migrating band cross-reacting with the anti-MITF antibody in the cells in which

MITF had been edited using CRISPR/Cas9, suggesting that at least some KO cells retained a low level of expression of a truncated form of MITF. A similar band has been observed in a previously published [76] human SKmel28 melanoma cell line in which MITF was edited using CRISPR/Cas9 to reveal that MITF deletion leads to up-regulation of a set of extracellular matrix genes. We then used CRISPR/Cas9 to knock out *TFE3* and *TFEB* alone and in combination in the parental B16/F10 cells as well as in the previously reported MITF KO (**Figure 5B)**. The knockout of each factor alone or in combination would enable us to mimic conditions where not all family members are expressed, for example under glucose limitation when MITF and TFEB are suppressed but TFE3 remains.

RNA-seq in biological triplicate of each cell line grown under standard culture conditions revealed a robust remodeling of the transcriptional landscape. Volcano plots of each KO compared to parental cells revealed a range of significantly (FC $\geq$2; *p*-value <0.05) upregulated or downregulated genes (**Supplemental Figure S4A-G)**. Notably, compared to the *MITF* KO (**Supplemental Figure S4A**), fewer genes were differentially expressed in the *TFE3* and *TFEB* single KOs (**Supplemental Figure S4B, C**), and the *MITF/TFEB* DKO (**Supplemental Figure S4F**) or the TKO (**Supplemental Figure S4G**) exhibited a greater number of differentially expressed genes, suggesting that some genes were regulated by more than one family member. A heatmap of the hierarchical clustering of RNA-seq of the parental cells and each KO cell line revealed a surprisingly complex gene expression pattern (**Figure 5C**). For ease of reference, gene expression clusters were labelled A-G and a full list of genes in each cluster and their relative expression in each KO cell line is provided in **Supplementary Table S2**.

Examination of the gene expression profiles reveals a number of interesting features. First, consistent with the Volcano plots (**Supplemental Figure S4A-G)** KO of *MITF* alone has a bigger impact than knockdown of either *TFEB* or *TFE3* alone: a range of genes within clusters A3 and C2 exhibit a greater upregulation in the *MITF* KO cells than in the *TFE3* or *TFEB* KO cells (**Figure 5C**). Moreover, the up-regulation of the MITF-repressed genes in cluster C2 is reversed in the MITF/TFEB DKO or the TKO, indicating that the up-regulation in the absence of *MITF* is driven by TFEB. Clusters B, D and F contain genes that are moderately downregulated in the *MITF* KO, but not in the single *TFE3* or *TFEB* KOs or in the *TFEB/TFE3* DKO. However, the down-regulation is amplified in the TKO, suggesting that all three factors may play a positive role in regulating this set of genes. In the *TFE3/TFEB* DKO gene expression was largely similar to that of the parental cells. However, more significant changes were noted when *MITF* was knocked out together with other family members. For example, in the *MITF*/*TFE3* DKO we observed enhanced up-regulation of a set of genes within clusters A1 and C1 compared to the *MITF* KO that were unaffected by KO *TFE3* alone. As the up regulation of cluster A1 and C1 genes was reversed in the TKO, this suggests that the presence of MITF and TFE3 can hinder the upregulation of genes in the A1 and C1 clusters by TFEB. Cluster G genes were much more up-regulated in the *MITF/TFEB* DKO than in any other KO, but were not up-regulated in the TKO, indicating that their expression is controlled by TFE3 in the absence of MITF and TFEB. Despite the complexity of the gene expression data, the results clearly show

that each member of the MITF family of transcription factors can in some cases compensate for another family member, and on some genes can have an opposing effect to other family members.

To gain an insight into the biological process regulated by MITF, TFEB and TFE3 we performed GSEA to highlight the enrichment of specific HALLMARK gene sets among those upregulated or downregulated by knockout of one or more MITF family members. To facilitate comparisons, we focus here on describing only a few of the differentially regulated gene sets. Compared to parental, the *MITF* KO exhibited an up-regulation of the EMT gene set and down regulation of G2M CHECKPOINT and E2F and MYC TARGETS, consistent with MITF low cells being slow-cycling and invasive [25,27] (**Figure 5D**). Also noted was an increase in expression of the HYPOXIA gene set, consistent with a previous report that $MITF^{Low}$ cells can exhibit high levels of succinate, an inhibitor of the prolyl hydroxylases that trigger Hypoxia-induced Factor (HIF) degradation [13]. In direct contrast, the *TFE3* KO (**Figure 5E**) exhibited up-regulation of the G2M CHECKPOINT, and MYC and E2F TARGETS gene sets, but no significant change in the EMT gene set. Both the GLYCOLYSIS and MTORC1 signaling gene sets were up-regulated in *TFEB* KO cells (**Figure 5F**) but were not significantly altered in either the *MITF* or the *TFE3* KOs. The EMT gene set was also upregulated in the *TFEB* KO, as it was in the *MITF* KO. The INTERFERON RESPONSE gene sets were down regulated in all three KOs. Like the *TFEB* KO, the *TFE3/TFEB* DKO (**Figure 5G**) also exhibited robust up-regulation of GLYCOLYSIS, as well as HYPOXIA and EMT, which were also up-regulated in the *MITF* and *TFEB* KOs, but downregulated or unchanged respectively in the *TFE3* KO. As in the *MITF* KO, the MYC and E2F TARGETS gene sets were downregulated in the *TFE3/TFEB* DKO (**Figure 5G**). Notably the up-regulation of MTORC1 SIGNALING in the *TFEB* KO (**Figure 5F**) was not observed in the *TFE3/TFEB* DKO (**Figure 5G**), suggesting the up-regulation of MTORC1 was dependent on intact TFE3. This is consistent with the down-regulation of MTORC1 signaling-associated genes in the *MITF/TFE3* DKO (**Figure 5H**), but not in the *MITF* KO (**Figure 5D**). Similarly, GLYCOLYSIS, that was strongly up-regulated in both the *TFEB* KO (**Figure 5F**) and the *TFE3/TFEB* DKO (**Figure 5G**), was only moderately changed in the *MITF/TFE3* DKO (**Figure 5H**) and was unchanged in the *MITF/TFEB* DKO (**Figure 5I**). These data suggest that glycolysis-related gene expression is up-regulated by MITF, but this role of MITF is largely counteracted by TFEB and to a lesser extent TFE3. The *MITF/TFE3* (**Figure 5J**) and *MITF/TFEB* (**Figure 5I**) DKOs also exhibit robust downregulation of the G2M CHECKPOINT, and E2F and MYC TARGETs gene sets. Thus, the enrichment of these gene sets observed in the *TFE3* KO (**Figure 5E**) is dependent on MITF expression. In addition, EMT is again robustly up-regulated in the *MITF/TFEB* DKO (**Figure 5I**), and in the TKO (**Figure 5J**), but not in the *MITF/TFE3* DKO (**Figure 5H**), with the TKO (**Figure 5J**) also exhibiting strong down-regulation of the MTORC1 SIGNALING, MYC and E2F TARGETS gene sets. One important conclusion from these experiments is that the TFE3 KO behaves very differently from that of the TFEB KO. This was substantiated by comparing the genes significantly differentially regulated by the TFE3 KO or TFEB KO in the MITF KO background. In this analysis, 906 genes were upregulated and 1015 genes downregulated in the MITF/TFEB DKO compared to the MITF/TFE3 KO (**Supplemental Figure S4H)**. GSEA analysis revealed robust upregulation of the

INTERFERON ALPHA and GAMMA RESPONSE gene sets as well as those associated with EMT and HYPOXIA. We also noted strong downregulation of mTORC1 signaling, MYC TARGETS, the UNFOLDED PROTEIN RESPONSE and OXIDATIVE PHOSPHORYLATION. The robust differential regulation of these gene sets is strongly indicative that TFEB and TFE3, in the absence of MITF, do not play the same role.

The more robust changes in gene expression revealed in the DKOs and TKO compared to the single KOs was reflected in changes in cell proliferation rate. After plating 4000 cells, cell counting based on CyQuant, a cell permeable DNA dye which directly reflects cell number independent of cellular metabolic status, revealed that proliferation was slightly reduced in the *MITF* KO, increased in the *TFE3* KO and was unaffected in the *TFEB* KO (**Supplemental Figure S4I)**. While the *TFE3/TFEB* DKO grew at a similar rate to the parental cells, the *MITF/TFE3* and *MITF/TFEB* DKOs exhibited severely reduced proliferation that was also impaired in the TKO. Note, however, that to establish cell lines, cells must proliferate and any more substantial effect of each KO on proliferation may therefore be suppressed. Nevertheless, these observations strongly suggest that TFEB and TFE3 can largely substitute for MITF in control of the cell cycle.

Differential metabolic impact of MITF family genes

One key observation from the GSEA was that MITF controls glycolysis-related gene expression. To determine whether the results of the GSEA were reflected in the metabolic activity of the cells we undertook Seahorse assays to determine the oxygen consumption rate (OCR) and extracellular acidification rate (ECAR), indirect measures of oxidative phosphorylation and glycolysis respectively, in the parental and MITF-family KO cell lines. The ECAR (**Figure 6A, left panel**) was lowest in the parental cells and was moderately increased in all KO cell lines, and especially in the TFE3 KO and MITF/TFEB DKO, with the TKO exhibiting the least increase. Treatment with oligomycin, an inhibitor of mitochondrial reversible ATP synthase that uncouples oxidative phosphorylation, revealed that all cells retained a glycolytic reserve that was largely proportional to basal glycolysis. Treatment with Rotenone and Antimycin A to block the electron transport chain had a moderate effect only in the TFEB/TFE3, MITF/TFE3 and TKO cell lines. Measurement of the OCR (**Figure 6A, right panel; Figure 6B**) revealed more dramatic differences between cell lines. While parental B16/F10 cells have a relatively low basal OCR, a striking increase was detected in the MITF KO as well as to a lesser extent in the MITF/TFE3 and the MITF/TFEB DKOs. As the TKO exhibited a substantially reduced increase in the OCR compared to the MITF KO, these data suggest first, that MITF suppresses oxidative phosphorylation, and second, that either TFEB or TFE3 alone in the absence of other family members may promote oxidative phosphorylation. These conclusions were supported when we examined the contribution of glycolysis or mitochondrial oxidative phosphorylation to ATP production (**Figure 6C**). The MITF KO produced 60% more ATP than the parental cells, with the most significant increase arising from mitochondrial ATP production; 37 % of total ATP production was derived from oxidative phosphorylation in parental cells compared to 53% in the MITF KO cells. This

suggests that MITF suppresses ATP production from oxidative phosphorylation. For the remaining KO cell lines, the ratio of mitochondrial to glycolytic ATP production was similar to the parental cells. However, the increased mitochondrial ATP production by the MITF KO cells was substantially reduced in the TKO, indicating that TFE3 or TFEB contribute to increasing ATP production in the MITF KO cells. Consistent with this, the MITF/TFEB and MITF/TFE3 DKO cells also exhibited reduced overall ATP production compared to the MITF KOs, and no significant increase in ATP production was noted in the TFEB/TFE3 DKO cells. Taken together, the results suggest that MITF supresses mitochondrial ATP production from oxidative phosphorylation and that much of the increase arising in the absence of MITF depends on TFEB and TFE3.

We next examined in the parental and KO cell lines expression of genes in the HALLMARK Oxidative Phosphorylation gene set. Notably many genes were upregulated in the *MITF* KO, but not in the *MITF*/*TFEB* DKO or the TKO (**Figure 6D**). The increased expression of these genes in the *MITF* KO is therefore largely dependent on *TFEB*. In the *MITF*/*TFE3* DKO, expression some genes, such as *Atp5d* or *Cpt1a*, were up-regulated similarly to the *MITF* KO, and were downregulated in the TKO, indicting a role for TFEB in their expression in the absence of MITF. However, expression of other genes, such as *Hadha* that was up-regulated in the *MITF* KO, were not increased in the *MITF*/*TFE3* KO. These data would again be consistent with elevated ATP production from oxidative phosphorylation in the absence of MITF being dependent on TFEB and TFE3.

Differential regulation of key target genes by the MITF-family

We next reviewed the effect of the KO of each MITF family member on their own mRNA expression. The *MITF* gene has multiple promoters driving expression of distinct isoforms in different cell types [9]. All three factors are able to bind the *MITF* gene (**Supplemental Figure S5A**) at the same 4 major locations upstream of the melanocyte specific MITF-M isoform, all with consensus binding sites (TCACATGA or ACACGTGA). Consistent with previous work that highlighted the ability of ectopic MITF to repress its own expression [13], *MITF* KO led to elevated *MITF* mRNA levels (**Supplemental Figure S5B).** The *MITF* KO also exhibited elevated expression of the *TFEB* and *TFE3* genes. However, no binding within the gene body or 5' regions by any MITF family member was detected in the vicinity of the *TFEB* and *TFE3* genes (**Supplemental Figure S5C, D**) and only one weak non-consensus binding site around 18 kb downstream from *TFEB* was identified. The moderate up-regulation of *TFEB* and *TFE3* expression in the *MITF* KO, is therefore likely indirect. However, the increased *MITF* mRNA in the *MITF* KO was abrogated in the *MITF/TFEB* DKO (**Supplemental Figure S5B**), suggesting that TFEB plays a positive role in regulating *MITF* mRNA expression in the absence of MITF. It is also likely that TFE3 positively contributes to *MITF* expression given the lower levels of *MITF* expression in the TKO compared to the *MITF/TFEB* DKO.

We next focussed our attention on a set of specific genes with relevance to melanoma biology (**Figure 6E**), all of which are known to be directly bound and regulated by MITF. These include many genes implicated production of melanin and formation or transport of melanosomes, melanocyte differentiation

functions. We also included two additional MITF targets, *Ppargc1a* [19,20], that promotes mitochondrial biogenesis and respiration, and *Scd1*, a key fatty acid desaturase required for melanoma proliferation [21]. The results were surprising.

All the selected genes have been reported to be positively regulated by MITF, yet in the *MITF* KO some of those implicated in melanocyte differentiation functions, such as *Mc1r*, *Dct*, *Tyrp1*, *Trpm1*, were up-regulated, while expression of others such as *Tyr*, *Pmel*, and *Slc45a* was largely unchanged (**Figure 6E**). Only *Mlana*, *Gpr143* and *Rab38a* were moderately downregulated. This suggests that MITF may play a role as a negative regulator of at least some of these genes, at least in proliferating B16 cells. This interpretation was confirmed using 501mel human melanoma cells in which ectopic murine MITF is expressed from a doxycycline-inducible promoter (**Figure 6F,G**). The result revealed that induction of MITF led to a reduction in expression of all differentiation-associated genes. By contrast, both *Scd* and *Ppargc1a* were upregulated as expected. These results indicate that at least at some differentiation genes MITF may play a negative regulatory role in proliferating melanoma cells. However, expression of all genes, including *Scd1* and *Ppargc1a,* were strongly downregulated in the MITF/TFEB DKO and the TKO (**Figure 6E**). Thus, in the absence of MITF, the induction of genes such as *Dct*, *Tyrp1*, and *Trpm1*, as well as the basal expression of the entire set of genes was largely dependent on TFEB, not MITF. Note that these genes are all bound by all three MITF family members. Example binding profiles for *TYR*, *MLANA* and *SCD* are shown in **Figure 3J**, and for *PMEL* in Supplementary **Figure 6E.**

Two other proliferation associated MITF target genes, *Cdk2* [16] and *Met* [77] are also bound by all three family members (**Supplemental Figure S5E)** and are similarly moderately down-regulated in the *MITF* KO (**Figure 6H)**, as well as in the *MITF/TFE3* and *MITF/TFEB* DKOs, and the TKO. However, *Met* is up-regulated in the *TFEB/TFE3* DKO but not in the single *TFEB* or *TFE3* KO cells. This is consistent with *Met* being upregulated by MITF, as previously described [77], with both TFEB and TFE3 contributing to its repression.

Recent evidence indicated that melanoma progression can be fuelled in MITF^{High} phenotype cells by uptake of long-chain fatty acids via fatty acid transporter proteins (FATPs) [78-80]. Inactivation of *MITF* has little effect on expression of *Slc27a1* (**Figure 6H),** that is bound by all MITF family members (**Supplementary Figure S5E)** and encodes FATP1, previously implicated in melanoma progression [78]. The *TFEB* KO also has a minimal effect. However, the *Slc27a1* gene is strongly downregulated in the *TFE3* KO (**Figure 6H)**, suggesting that it is TFE3 that plays a key role in its regulation rather than MITF or TFEB. By contrast the *Sesn2* gene, encoding a negative regulator of mTORC1 [81-84], is strongly upregulated in the *MITF* KO, consistent with MITF's pro-proliferative role (**Figure 6H)**. However, it is downregulated in the *TFE3* KO and in the TKO. As *SESN2* is bound downstream by all three MITF family members at a consensus TCACGTGG motif (**Supplementary Figure 5E)**, this result suggests that TFE3 may mediate the elevated *SESN2* expression in the *MITF* KO. A similar pattern of expression was observed for the *DDIT3* gene, encoding the ATF4-regulated pro-apoptotic transcription factor CHOP [85,86]. However, no

binding was observed to *DDIT3* by any member the MITF family, suggesting that the regulation observed is indirect.

AXL, expressed in MITF^{Low} melanoma cells and encoding a key receptor tyrosine kinase linked to therapy resistance [28,29], is also not bound by any MITF family member, but is strongly upregulated in the *MITF*/*TFEB* DKO (**Figure 6H)**. However, as expression in the TKO is similar to parental cells, the increased expression observed in the *MITF*/*TFEB* DKO must arise through an effect of TFE3.

Differential regulation of interferon alpha response and collagen genes by MITF family members

Over recent years there has been increasing interest in how the extracellular matrix signals in melanoma, and specifically in how signalling via integrins can promote therapy resistance. For example, in vivo, BRAF inhibition can drive formation of a drug-tolerant microenvironment via integrin signalling to FAK [87]. Importantly, it has recently been revealed that MITF can reprogram the extracellular matrix by repressing ECM-associated genes and focal adhesion pathways [76,88]. We therefore examined expression of a set of collagen genes as well as the procollagen-lysine,2-oxoglutarate 5-dioxygenase 1 and 2 genes (*PLOD1* and *PLOD2*) that are required for generation of hydroxylysyl groups that is critical for the stability of intramolecular collagen crosslinks.

For *PLOD1*, expression was increased in the *MITF* and *MITF/TFE3* DKO, but not in the *MITF/TFEB* DKO or TKO **(Figure 6I**), indicating that TFEB maybe up-regulating *PLOD1* expression in the absence of MITF and TFE3. Similar results were obtained for *COL4A1*, but for *COL18A1*, while no increase was seen in the *MITF* KO, expression was robustly upregulated in the *MITF/TFE3* DKO but not in the TKO. Again, these data point to upregulation of *COL18A1* by TFEB in the absence of MITF and TFE3. *PLOD1*, *COL4A2* and *COL18A1* are bound by all MITF family members, consistent with their regulation being direct.

COL5A1 and *COL6A1* are also bound by all MITF family members but exhibit a different pattern of regulation in which expression is elevated in the *MITF/TFEB* DKO, but is maintained in the TKO **(Figure 6I**). This would be consistent with repression by either MITF or TFEB, but positive regulation in the absence of these factors is not mediated by TFE3. Notably a similar pattern of expression was observed for *COL4A1*, *COL5A3* and *COL6A1*, but none of these genes are bound by any MITF family member. Thus, KO of MITF family genes can lead to indirect, deregulated expression of collagen genes.

Finally, a third set of collagen genes, *COL8A1* and *COL11A1,* bound by all three MITF family members, and *COL1A1* and *PLOD2* that are not bound, are only upregulated in the *MITF/TFEB* DKO but not in the TKO **(Figure 6I**). This indicates that TFE3 is required to increase their expression in the absence of MITF and TFEB. *COL1A2*, which is also not bound, exhibits a similar pattern of expression, but is upregulated in the *MITF* KO as well as the *MITF/TFEB* DKO.

The dramatic differences in regulation of specific genes by different MITF family members was also noted in the HALLMARK Interferon Alpha gene set (**Supplemental Figure S5F**). Here, many genes were down-regulated in the *MITF* KO but were strongly upregulated in the *MITF*/*TFEB* DKO with the increase being abolished in the TKO. This suggests that for those genes MITF plays a role in their basal expression,

but that in the absence of MITF and TFEB their expression is positively regulated by TFE3. Many are also bound by MITF family members (**Supplemental Table S3**), and expression of *CD47*, best known as a 'don't-eat-me' signal [89], is robustly upregulated in the MITF/TFEB DKO but not in the TKO, and all three family members bind downstream (**Supplemental Figure S5G**). Thus, under stress conditions when MITF and TFEB are suppressed, TFE3 may promote expression of genes within the HALLMARK Interferon Alpha gene set to modulate the immune microenvironment.

Taken together the results highlight how different MITF family members, alone or in combination, exert fundamentally different direct and indirect effects on key genes even though for those genes that are bound, all family members exhibit similar binding in WT cells.

TFEB and TFE3 are required for efficient tumor growth in vivo

The results so far have revealed a complex role for MITF family members in that while all bind a similar set of target genes, they act alone and in combination to differentially regulate genes. To assess their role tumorigenesis in vivo, we compared the tumor forming ability of each single KO to the parental B16 cells in C57BL/6 mice following subcutaneous transplantation. The results obtained revealed that tumor formation by the *MITF* and *TFE3* KO cells was significantly delayed compared to parental cells (**Figure 7A-C**). The *TFEB* KO cells also grew more slowly than the parental cells. Finally, we also assessed the ability of the parental and KO cells to colonize the lungs following tail vein injection. In this assay, lung colonization was severely reduced in the *MITF* KO, but was less affected in the *TFEB* and *TFE3* KO cells (**Figure 7D, E**). In summary, TFE3 and to a lesser extent TFEB, can affect tumor growth in vivo and proliferation in vitro even in cells expressing other family members, while loss of *MITF* severely compromises tumor formation and cell proliferation.

Discussion

Whether apparently functionally identical transcription factors with identical DNA binding specificity might perform distinct functions at the same target genes is a key question that is especially relevant to cancer where the adaptive response to stress underpins disease progression and therapy resistance. Here we explored the function in melanoma of MITF, TFE3 and TFEB, three highly related transcription factors with identical DNA binding domains.

Since it was first identified [90], the *MITF* gene has emerged as a major coordinator of many key aspects of melanoma biology [9]. Importantly, MITF is transcriptionally and translationally downregulated by the integrated stress response leading to dedifferentiation, reduced proliferation and a switch to invasion [10]. Yet while the role and regulation of MITF has been a focus for understanding how phenotypic transitions in melanoma are implemented, the potential for the other MITF family members, TFEB and TFE3, to contribute to any adaptive response has been understudied. In part, this is because unlike many other tissue types where only TFEB and/or TFE3 may be expressed, the melanocyte-specific isoform of MITF, that is not inhibited by mTORC1, is largely constitutively nuclear [91]. Here we have taken steps to decipher the

complex relationship between MITF, TFE3 and TFEB in melanoma and have provided several novel and surprising insights.

First, we found that depletion of MITF led to a reduction in mTORC1 signaling. MITF appears to control mTORC1 activity via a range of mechanisms including by suppressing expression of *PTEN* and the negative mTORC1 regulator *SESN2*. This makes sense since MITF can promote proliferation and consequently $MITF^{Low}$ cells tend to be slow-cycling [25,27], meaning that they do not require high levels of protein synthesis to support reduced proliferation. Moreover, MITF also controls the expression of *FNIP2* and *RRAGD*, two factors implicated in mTORC1 signalling to TFEB/TFE3 [49,50,58,92]. However, surprisingly we found that in $MITF^{High}$ melanoma cells TFEB and TFE3 were both largely nuclear under steady state conditions, with mTOR inhibition leading to increased levels of nuclear protein. Signalling downstream from mTORC1 is partitioned into canonical signalling, in which substrates like S6K are subject to RHEB-dependent phosphorylation, and a non-canonical pathway where TFEB and TFE3 recognition by mTORC1 is dependent instead on RAGC/D and FLCN/FNIP2 [93]. Paradoxically, mutations leading to activation of mTORC1 can trigger a negative feedback loops that can lead to hypo-phosphorylated and nuclear TFEB/3 [94,95]. One possibility is that MITF, in promoting proliferation and canonical mTORC1 signaling, may suppress non-canonical signalling leading to increased nuclear TFEB and TFE3. In this respect, the constitutively nuclear TFEB and TFE3 found in $MITF^{High}$ lines is reminiscent of the constitutive nuclear localization of TFEB observed in pancreatic adenocarcinoma (PDAC) [53]. Alternatively, and perhaps more likely, dimerization between TFEB/TFE3 in melanoma cells with the non-mTORC1-regulated melanocyte-specific isoform of MITF that would not be expressed in many other cell types used to study TFEB/TFE3 could lead to the increased nuclear/cytoplasmic ratio observed in $MITF^{High}$ cells.

Even more surprising was the observation that TFE3 is cytoplasmic in IGR39 cells in which RAGD is not expressed. Again, one possibility is that in these cells, rather than cytoplasmic retention, it is increased nuclear export that might be crucial in controlling TFE3 subcellular localization. Collectively these data would suggest that the regulation of TFE3/TFEB factor cytoplasmic nuclear shuttling in melanoma cells may be different from that seen in many cell types previously used to examine regulation of these transcription factors. However, the molecular mechanism underpinning their regulation in melanoma warrants further investigation.

Second, our results reveal that in response to glucose limitation there is a dramatic remodelling of MITF family expression (**Figure 7F**). MITF is downregulated, in agreement with previous observations [11] and TFEB is dephosphorylated before also being downregulated. In principle, TFEB dephosphorylation may arise in part owing to reduced MITF expression leading to a reduction in FNIP2 and RAGD expression, previously reported to be required for TFEB phosphorylation by mTORC1 at the lysosome [58,92,96], but also because glucose limitation inactivates the TFEB nuclear export signal [67]. Finally, once MITF and TFEB are downregulated, TFE3 remains as the sole MITF family member present in nutritionally stressed melanoma cells where it acts to suppress cell death. The TFEB to TFE3 switch is not limited to melanoma cells, as we show it also operates in colon cancer cells, and we view it as likely that it will operate in many

if not all cell types where TFEB and TFE3 have an extensive role in cell and tissue homeostasis [33,47]. Indeed, in macrophages, where TFEB and TFE3 cooperate to control inflammatory signalling [41], lipopolysaccharide treatment leads to an initial activation of TFEB before its expression is lost, leaving TFE3 as the sole family member expressed. The glucose deprivation-induced switch from TFEB to TFE3 may also be relevant to the ability of these factors to be activated by AMPK independently of mTORC1 [97].

Third, the interpretation of the MITF-family cascade should be made in the context of our observation that, against expectation, TFEB and TFE3 are not equivalent: while our ChIP-seq analysis revealed that all three MITF family members bind the same repertoire of genes, their actions on those genes, alone or in combination are radically different. This is important since several studies have shown that at many genes TFE3 and TFEB appear to play an equivalent role and many studies use *TFEB*/*TFE3* DKOs. Instead, our results highlight that each factor makes a unique contribution, with GSEA suggesting that TFEB plays broadly similar role to MITF, but that TFE3 instead acts in opposition to TFEB, at least at some target genes. Our conclusion is that in non-stressed conditions, MITF will promote proliferation but that on encountering microenvironmental stresses, such as limitation in glucose supply, MITF will be downregulated via the ISR. On loss of MITF, TFEB will transiently take on MITF many functions to buy time for cells to resolve the stress. If the stress remains unresolved, TFEB is also suppressed, and TFE3 then will promote a gene expression program compatible with cell survival, including up-regulation of many interferon alpha response genes, including the CD47 'don't-eat-me' signal.

Fourth, MITF has been widely assumed to be the key regulator of melanocyte differentiation genes. Instead, we find that a number of differentiation-associated genes are upregulated on *MITF* KO and downregulated if MITF is overexpressed. The upregulation in the MITF KO cells was dependent on TFEB which has not previously been implicated in melanocyte/melanoma differentiation. Notably in the same *MITF* KO cells a number of pro-proliferative MITF targets such as *Cdk2* and *Met* are down regulated. We hypothesize that in proliferative cells MITF may play a positive role in regulating pro-proliferation genes, but at the same time it will suppress TFEB-driven activation of differentiation genes; by contrast, in differentiated cells, MITFs function will likely be reversed, upregulating differentiation genes and suppressing those driving cell division. The nature this switch is currently unknown, but may be related to regulation of MITF's interaction with co-factors by proliferation-associated post-translational modifications such as acetylation [62,69].

Previous work on TFEB in melanoma has provided some interesting, but in some cases, apparently conflicting observations. For example, knockdown of TFEB in murine melanoma cells using shRNA supported a role for TFEB in promoting melanoma proliferation, including reduced proliferation associated with lower glucose and glutamine uptake and consequently reduced glycolysis, glutaminolysis and slower tumor growth in vivo [56]. By contrast, Li et al [98], who reported that BRAF inhibition led to increased TFEB-promoted autophagy, showed that ectopic expression of a constitutively active TFEB S142A mutant led to tumors growing more slowly, whereas an S142E phosphomimetic mutant increased metastatic. Our results are more in line with those of Ariano et al [56] since we observed moderately reduced tumor growth in the

single B16 *TFEB* KOs, although very little change in proliferation was noted in vitro unless *TFEB* was also knocked out together with *MITF*. Our GSEA also revealed increased mRNA expression of glycolysis genes in the *TFEB* KO that was not present in the *MITF/TFEB* DKO. We view it likely that the increase in MITF-dependent expression of glycolysis-associated mRNAs in *TFEB* KO cells represents a mechanism aiming to compensate for the decreased glucose uptake and activity of glycolysis enzymes observed by Ariano et al [56] in shTFEB-expressing cells. Notably we also reveal greatly increased ATP production in the *MITF* KO that is derived largely from increased oxidative phosphorylation and which is dependent on TFEB and TFE3. This is consistent with slow-cycling melanoma cells, which are $MITF^{Low}$ [27], exhibiting elevated oxidative phosphorylation [99,100]. However, other studies have suggested that MITF, through its ability to up-regulate *PPARGC1A*, can increase oxidative phosphorylation in part through increased mitochondrial biogenesis [19,20]. In agreement with these reports, our results indicate that *PPARGC1A* expression is indeed up-regulated by MITF overexpression. However, in the *MITF* KO it is also upregulated, with the increased expression dependent on TFEB. These data strongly implicate TFEB and TFE3 as playing a key role in the metabolic switch associated with loss of MITF, for example under glucose limitation conditions.

Limitations of this study

It is clear that MITF, TFE3 and TFEB bind the same sites in a similar repertoire of genes, and that some target genes are differentially regulated by each family member. However, since each family member can both homo- and heterodimerize, we cannot know how much of their capacity to dictate specific gene expression programs is mediated by heterodimerisation. Moreover, as the ChIP-seq was performed only in WT cells, it is possible that loss of MITF and TFEB, for example on glucose limitation, could lead to chromatin remodelling and acquisition of novel recognition sites for TFE3, as recently noted in TFEB-negative SKmel28 cells [101]. If this also occurs in the *MITF* KO cell lines used here, it is possible that at least some genes regulated by TFE3 and TFEB but not bound in our ChIP-seq may be bound in the absence of MITF. In other words, we may be underestimating the numbers of genes directly regulated by MITF family members. Moreover, the differential gene expression observed here for the single, double or triple KO cell lines grown in vitro may not necessarily reflect the expression that may occur on transient loss of expression in vivo when cells are subject to stresses such as nutrient limitation or inflammatory signalling. In part this is because KO cell lines are selected for proliferation and consequently cells must bypass any major block to proliferation induced by the KO. By contrast, in vivo there is no imperative to proliferate beyond that imposed by the expression of activated oncogenes such as *BRAF*. However, even with an activated oncogene, proliferation in vivo is strictly dependent on a sufficient supply of nutrients. The differential gene expression observed here using the KO cell lines should therefore be regarded as indicating the potential of the MITF family members, alone or in combination, to differentially regulate gene expression.

Materials and Methods

KEY RESOURCES TABLE

REAGENT or RESOURCE	SOURCE	IDENTIFIER
Antibodies		
Mouse monoclonal anti-MITF (C5)	Abcam Cat# ab12039	RRID: AB_298801
Mouse monoclonal anti-GAPDH (6C5)	Santa Cruz Biotechnologies Cat# sc-32233	RRID: AB_627679
Mouse monoclonal anti-PTEN (2F4C9)	ThermoFisher Scientific Cat#32-5800	RRID: AB_2533087
S6	Cell Signaling Cat#2217	RRID: AB_331335
pS6	Cell Signaling Cat#2211	RRID: AB_331679
ACTIN (AC-40) mouse monoclonal	Sigma-Aldrich Cat# A4700	RRID: AB_2560935
RRAGD	Cell Signaling Cat# 4470	RRID: AB_1950380
FNIP2	Cell Signaling Cat#57612	RRID: AB_2799530
TFEB Hs	Cell Signaling Cat# 4240	RRID: AB_11220225
TFE3	Sigma-Aldrich Cat# HPA023881	RRID: AB_1857931
TFE3 (for Immunofluorescence)	Cell Signaling Cat#37785S	RRID: AB_2799119
TFEB Mm	Cell Signaling Cat# 83010	RRID: AB_3105800
HA	Roche Cat#11666606001;	RRID: AB_514506
HA	Sigma-Aldrich Cat#H3663	RRID: AB_262051
HA	Cell Signaling Technology Cat#2367	RRID: AB_2314619
ERK 2	Santa Cruz Biotechnology Cat#sc-153	RRID: AB_2141293
ERK 2	Santa Cruz Biotechnology Cat#sc-1647	RRID: AB_627547
GAPDH	Santa Cruz Biotechnology Cat#sc-32233	RRID: AB_627679
Anti-Mouse Alexa Fluor 488	ThermoFisher Scientific Cat#A11001	RRID: AB_2534069
Anti-Mouse Alexa Fluor 546	ThermoFisher Scientific Cat#A10036	RRID: AB_11180613
Anti-Rabbit Alexa Fluor 488	ThermoFisher Scientific Cat#A11008	RRID: AB_143165
Anti-Rabbit Alexa Fluor 546	ThermoFisher Scientific Cat#A10040	RRID: AB_2534016
Alexa Fluor 488 donkey anti-rabbit IgG (H+L)	I ThermoFisher Cat#A21206	RRID: AB_2535792
Bacterial and Virus Strains		
Subcloning Efficiency DH5α bacteria	Invitrogen Cat#18265-017	

Biological Samples		
Chemicals, Peptides, and Recombinant Proteins		
Torin	Cayman Chemicals	Cat# 10997
Geneticin	Gibco	Cat# 10131027
Puromycin	Gibco	Cat# A1113802
Doxycycline	Sigma-Aldrich	D9891
DMSO	Sigma-Aldrich	D2650
DAPI		
Doxycycline	Sigma	Cat#D9891-10G
cOmplete™ ULTRA Protease Inhibitor Cocktail	Sigma	Cat# 5892988001
Glutamax DMEM media	GIBCO	Cat#31966021
RPMI 1640 media	GIBCO	Cat#21875-034
HBSS	GIBCO	Cat#21090-022
DMEM	GIBCO	Cat#11965
RPMI NO GLUCOSE	GIBCO	Cat#11879-020
DMEM no glucose	GIBCO	Cat#11966-025
Normal Fetal Bovine Serum	Sigma	Cat#F4135
Lipofectamine CRISPRMAX	Invitrogen	
OptiMem	GIBCO	Cat#31985-062
FuGENE6	Promega	Cat#E2692
BSA	Sigma	Cat#A9647-100G
Lipofectamine RNAiMAX	Invitrogen	
Sodium Azide	Sigma	Cat#S2002
Critical Commercial Assays		
ECL detection kit	Amersham Biosciences	Cat#GE Healthcare, RPN2106
RNA extraction RNeasy Mini Kit	Qiagen	Cat#74106
MycoAlert™ mycoplasma detection kit	Lonza	Cat#LT07-318
PureLink™ Genomic DNA Mini Kit	Invitrogen	Cat# K182002
QIAprep Spin Miniprep Kit	QIAGEN	Cat# 27106
Deposited Data		
RNA-seq from MITF, TFEB and TFE3 B16 KO cell lines	GEO	GSE270594
RNA-seq from 501mel cell lines	GEO	GSE277250
TFEB ChIP-seq	GEO	GSE270585
TFE3 ChIP-seq	GEO	GSE270590
shMITF RNA-seq:	GEO	GSE255256
RNA-seq from inducible CTNNB1 in IGR37 cells	GEO	GSE136803
Experimental Models: Cell Lines		
IGR37 Human melanoma cell line (female)	Obtained from Luisa Lanfrancone	[102]
IGR39 Human melanoma cell line (female)	Obtained from Luisa Lanfrancone	[102]
501mel Human melanoma cell line (female)	Obtained from Ruth Halaban, Yale	[103]
A375M Human melanoma cell line (male)	Obtained from ATCC	[104,105104,105104,105]
SKmel28 Human melanoma cell line (male)	Obtained from ATCC	[104]

SKmel30 Human melanoma cell line (female)	Obtained from ATCC	[106]
HBL Human melanoma cell line (female)	Obtained from Ghanem Lab, Brussels	[107]
WM793 Human melanoma cell line	Obtained from the ATCC	[108,109108,109]
WM266.4 Human melanoma cell line	Obtained from the ATCC	[110]
WM115 Human melanoma cell line	Obtained from the ATCC	[110]
WM9 Human melanoma cell line	Obtained from the ATCC	[111; 109]
MeWo Human melanoma cell line	Obtained from the ATCC	[112]
CHL-1 Human melanoma cell line	Obtained from the ATCC (Derived from RPMI 7932 cells)	Patent US5017478A
HT-29 Human Colon Cancer	Obtained from the ATCC	[113]
B16F10-Luciferase mouse melanoma cell line	Obtained from Luis Sanchez del Campo	[75]
B16F10-Luciferase MITF KO mouse melanoma cell line	Obtained from Luis Sanchez del Campo	[75]
Oligonucleotides		
siRNA control	Qiagen	Cat#1027281
siRNA MITF 1 5′-AAAGCAGTACCTTTCTACCAC-3′	Sigma	[10]
siTFE3	Santa Cruz	Cat#sc-38507
TFEB sgRNA 5′-AGTACCTGTCCGAGACCTAT	ThermoFisher A35533 CRISPR775049_SGM	This paper
TFE3 sgRNA 5′-GGTACTGTTTCACCTGCTGC	ThermoFisher A35533 CRISPR381077_SGM	This paper
Tfeb sgRNA 5′-TGGACACGTACTGTCCACCT	ThermoFisher A35533 CRISPR557759_SGM	This paper
Tfe3 sgRNA 5′- AGCGTGTAGGGTTCTCGAGG	ThermoFisher A35533 CRISPR284202_SGM	This paper
Recombinant DNA		
Plasmid Piggybac expression system		[114]
Software and Algorithms		
MetaQuant		[115]
ImageJ	https://imagej.nih.gov/ij/	
Cutadapt		[116]
STAR		[117]
Homer		[118]
EdgeR		[119]
TreeView		[120]
javaGSEA v.4.3.2		[121]
fastqc v.0.11.9		GitHub - s-andrews/FastQC
trim_galore v.0.6.5		[116]
clusterProfiler v4.6.2		Bioconductor
DOSE v3.24.2		Bioconductor

enrichplot v.1.18.4		Bioconductor
VennDiagram v.1.7.3		cran.r-project.org
ggplot2 v.3.4.4		cran.r-project.org
GraphPad Prism 7	https://www.graphpad.com	
Perseus		[122]
Other		

Cell lines

All human melanoma cell lines were grown in Roswell Park Memorial Institute (RPMI) medium, except HBL which were grown in Dulbecco's Modified Eagle Medium (DMEM), supplemented with 10% Fetal Bovine Serum (FBS), 50 units/mL penicillin and 50 units/mL of streptomycin. All human melanoma cell lines contain the $BRAF^{V600E}$ oncogenic mutation, except HBL and CHL-1 cells which possess wild-type BRAF. The mouse melanoma cell line B16/F10 was grown in DMEM, supplemented with 10% FBS as well as 50 units/mL penicillin and 50 units/mL of streptomycin. All cells were grown as a monolayer, and passaged once they reached around 80%-90% confluency.

For cell lines stably-transfected with PiggyBac doxycycline-inducible expression vectors, selection and maintenance was performed via the addition of 1 mg/mL of geneticin (G418) and 1 µg/mL of puromycin. Selection was first performed with geneticin for the first week, any live cells then allowed to recover until the second weekly selection treatment with puromycin. Cells were kept at 37 ºC with 10% CO_2 and grown in T75 culture flasks.

All cells were subject to authentication using STR analysis using Eurofins authentication service, and routinely tested by mycoplasma via PCR, following a previously established and published protocol [123] or use of the MycoAlert PLUS Mycoplasma Detection Kit (Lonza). Only mycoplasma-negative cells were used.

Cell fractionation

Cells were grown to approximately 70-80% confluency. Subcellular fractionation was performed using the Rapid, Efficient And Practical (REAP) method. Briefly, cells were washed in ice-cold 1X PBS before being scraped into 200 µL of ice-cold 1X PBS containing 0.1% NP-40 (1 tablet of the cOmplete Protease Inhibitor Cocktail (Roche, Cat No. 11697498001) and 1 tablet of the PhosSTOP Phosphatase Inhibitor Cocktail (Roche, Cat No. 4906837001) were added immediately before use) and triturated 5 times using a Gibson P200 pipette. After, 60 µL was removed and transferred to a 1.5 mL Eppendorf tube labelled 'whole cell fraction'. The remaining 140 µL was centrifuged using a table-top centrifuge (10 sec, 5000xg, 4 °C). After centrifugation, 60 µL of the supernatant was removed and transferred to a 1.5 mL Eppendorf tube labelled 'cytoplasmic fraction'. The remaining supernatant was removed, leaving only the insoluble pellet. The pellet was washed by resuspending in 200 µL of ice-cold 1X PBS

containing 0.1% NP-40 before centrifuging using a table-top centrifuge (10 sec, 5000xg, 4 °C). The supernatant was removed and discarded before resuspending the pellet in ice-cold 1X PBS containing 0.1% NP-40 and labelled 'nuclear' fraction. The 'whole cell' and 'nuclear' fractions were sonicated for 30 sec at 4 °C. After, 20 µL of 4X Laemmli buffer was added to all samples before boiling at 95 ºC for 5 min. All samples were stored at -20 °C.

Cell Cycle and DNA fragmentation analyses

Cells were transfected with 20 nM siRNA (siTFE3 #sc-38507, siMITF (QIAGEN, custom siRNA sequence: AAAGCAGUACCUUUCUACCAC or siCTRL (QIAGEN # 1027281)), in case of further treatments (-Glc) for another 6 h before samples collected in 1.2 ml DPBS (no Mg^{2+}/Ca^{2+}) + 5% FBS and fixed in 70% EtOH with gentle shaking at 4°C, 1 h. Cells were stained in 250 µl staining solution (DPBS + 0.5 mg/ml PI, 100 µg/ml (ThermoFisher P3566) RNAseA (Roche10109169001), 0.05% Triton X-100) at 37°C, 45'. Following one wash in 1 ml PBS, cells were resuspended in Resuspended in 250-500 µl DPBS + 5% FBS and analysed on flow cytometry (SONY MA900). Cell cycle were profiled using FlowJo (v10.8.1 for siTFE3 and v10.10.0 for siMITF) using Watson model (for siTFE3) and Dean-Jett-Fox model (for siMITF). DNA fragmentation (sub-G1 population) were defined as population with PI signals below the G1 for siTFE3 or directly from Dean-Jett-Fox model fitting.

CRISPR/Cas9 Knock-Out of TFEB and TFE3

For the *TFEB* and *TFE3* genes the top 10 most efficient sgRNAs in terms of on- and off-site efficacy identified using the Broad Institute Benchling software were evaluated using the Integrated DNA Technologies (IDT) Cas9 Checker software to choose the most efficient gRNA from the list. To generate target gene knockout cell lines, the Lipofectamine CRISPRMAX method (ThermoFisher) was followed. Cells were plated on Day 0 and allowed to adhere in a 6-well plate to reach 35% confluency at the moment of transfection on Day 1. 125 µl of Opti-MEM, 6.25 µg of Cas9 nuclease, 1.2 µg of synthetic gRNA and 12.5 µl of Cas9 Plus reagent were added to Tube 1 in that order and allowed to incubate at room temperature. The sequences of the guides were: TFEB - AGTACCTGTCCGAGACCTAT; TFE3 - GGTACTGTTTCACCTGCTGC; Tfeb – TGGACACGTACTGTCCACCT; Tfe3 – AGCGTGTAGGGTTCTCGAGG. Meanwhile, in Tube 2, 125 µl of Opti-MEM was gently mixed with 7.5 µl of CRISPRMAX reagent and incubated for no more than 3 min. The Lipofectamine mix was then added to the Cas9-gRNA ribonucleoprotein (RNP) complex, mixed well by pipetting, and incubated for 15 min at room temperature. Finally, fresh medium was added to the 6-well plate and the 250 µl lipofectamine-RNP complex mix was added to each well in a dropwise manner. Cells were then incubated a further 24-48 h before screening for monoclonal knockouts. Cells were trypsinized, collected into fresh medium in 5 mL total of suspension, counted using an automated counter and diluted accordingly until reaching about $5x10^5$/ml. At this point, cells were serially diluted into a final 1 ml suspension containing about 1000 cells. Clones were distributed into a 96-well plate, with an estimated density of 0.96 clones per well in a final

volume of 200 µl and left to grow for about 2 weeks or until visible colonies arising from single clones were seen. At this stage, cells were trypsinized and expanded until enough material could be obtained for Western Blotting to validate the monoclones. Secondary confirmation of knockout status was performed by extracting genomic DNA from monoclones and sending the PCR-amplified target sequence for Sanger sequencing, provided as a service from Eurofins, to ascertain the genomic event that occurred as a result of the Cas9 nuclease cutting the genome at the gRNA target site.

Western Blotting

Whole cell lysate was prepared by adding an appropriate amount of 1x Laemmli Sample Buffer (62.5 mM Tris-HCl, pH 6.8, 2% Sodium Dodecyl Sulfate, 10% glycerol, 5% ß-mercaptoethanol, 0.01% bromophenol blue) directly to the cells in the plate, usually 200 µl for one well of a 6-well plate at 80%-90% confluency. The whole lysate was then transferred to a 1.5 mL Eppendorf tube and boiled at 95 ºC for 10 min before analysis. 5%-10% of the total sample was used in each lane.

Proteins were analyzed via sodium dodecylsulphate polyacrylamide gel electrophoresis (SDS-PAGE) using 10% acrylamide from a 30% stock solution with 37.5:1 acrylamide to bis-acrylamide ratio (Severn Biotech). To allow fine resolving of specific phosphorylated proteins from their non-phosphorylated counterpart, an acrylamide stock with a ratio of 200:1 acrylamide to bis-acrylamide was used (Severn Biotech).

Samples were run/separated at 140V for 90 min in 1x Running Buffer (25 mM Tris, 192 mM glycine, 0.1 % SDS). Precision Plus Dual-Colour Standard (BioRad) was used as indicated by the manufacturer was used as a size marker. After SDS-PAGE proteins were transferred unto a nitrocellulose membrane (GE Amersham) in a wet transfer tank (BioRad) filled with 1x Transfer Buffer (25 mM Tris, 192 mM glycine, 20 % ethanol) and transferred at a constant amperage of 400 mA for 75 min. Membranes were then placed in 50 mL Falcon tubes and blocked at room temperature for 60 min in 5% Bovine serum albumin (BSA) in Tris buffered saline (TBS) containing 0.1% Tween (TBS-T). Membranes were then briefly rinsed with TBS-T before proceeding to primary antibody incubation, also performed in 5% BSA in TBS-T. Most primary antibodies were used in a 1:1000 dilution while housekeeping antibodies were diluted 1:5000. Overnight incubation with primary antibodies was performed by leaving the 50 mL Falcon tubes rolling and incubating in the cold room at 4 ºC. The following day, membranes were rinsed twice for 10 min before incubation with HRP-conjugated secondary antibodies diluted 1:5000 in 5% milk in TBS-T at room temperature for 120 min. Afterwards, membranes were again rinsed and washed 2 times for 10 min, at which point enhanced chemiluminescence reagent (ECL, GE Amersham) was incubated on the membranes for 5 min before the membranes were exposed to X-ray film (Fujifilm) and developed.

Immunofluorescence

For immunofluorescent experiments, cells were plated on circular glass coverslips (VWR) and grown until reaching 70-80% confluency in 24-well plates. Medium was aspirated and cells washed with 1x PBS at

room temperature and then fixed on the plate with 4% paraformaldehyde (PFA) in 1x PBS for 10 min at room temperature. After fixation, PFA was aspirated and coverslips rinsed 3 times with PBS followed by permeabilization with 0.2% Triton X-100 in PBS at room temperature for 10 min with agitation on a shaker. Permeabilization buffer was then aspirated and fresh PBS was added to the wells to rinse the fixed cells on the coverslips before blocking for 1 h at room temperature with 4% BSA in PBS in a shaker. Afterwards, coverslips were, dried and placed face down on a PARAFILM M (Sigma) sheet with 50 µl of primary antibody solution, consisting of primary antibody normally diluted 1:100 in 4% BSA in 1x PBS. Antibody incubation was either performed for 2 h at room temperature or overnight at 4º C, depending on affinity, concentration and ultimate signal obtained using the primary antibody. Coverslips were then placed into in a new sterile 12-well plate and washed 3x with PBS for 5 min each, before simultaneous incubation with secondary antibodies and DAPI, diluted both 1:500, face down in the parafilm with a light-protective cover. Once the secondary incubation was complete, coverslips were again transferred to a plate and washed with PBS for 5 min 3x times, dried and finally mounted on glass microscope slides (VWR) with MOWIOL (Millipore) mounting medium. Images were then taken with a confocal Zeiss LSM710 or LSM980, with image acquisition performed with the matching proprietary Zen software (Zeiss). Image processing was for presentation and publication purposes was done via Photoshop. Antibodies used are listed in Reagents in a later subchapter of this section.

Proliferation/survival assays

A DNA content-based cell proliferation assay that is independent of cellular metabolic status was carried out using CyQUANT™ Direct Cell Proliferation Assay (ThermoFisher, # C35011) as per manufacturer protocol using media only for background subtraction. To determine whether TFE3 promoted cell survival in low glucose, cells were plated in DMEM, transfected with 20 pm of a pool of 3 specific TFE3 siRNAs (SCBT #sc-38507) for 48 h before being placed in glucose free DMEM. Cells were then processed for flow cytometry using a SONY MA900 flow cytometer and subject to Dean-Jett-Fox analysis using FloJo.

Seahorse analysis

The oxygen consumption rate (OCR) and extracellular acidification rate (ECAR) were measured using a Seahorse XFe96 extracellular flux analyzer (Seahorse Bioscience, North Billerica, MA, USA). Briefly, 7,000-14,000 B16F10 cells were seeded in XF96 well plates with the objective of achieving approximately 75% confluence and homogeneous distribution. On the following day, the medium was replaced with fresh Seahorse XF medium without phenol red supplemented with 1 mM pyruvate, 2 mM glutamine, and 10 mM glucose and incubated one hour in a CO_2-free incubator to guarantee precise measurements of extracellular pH. Metabolic activity was analyzed using an Agilent Seahorse 96XF device using Real-Time ATP assay kit (Kit 103592-100) performed as described in the manufacturer's protocols. Respiratory parameters were calculated using the Seahorse Wave Desktop Software (Agilent Technologies). Values were normalized to

cell number. For the quantification and statistical analysis three or more independent repeats were performed for each experiment unless stated otherwise in the figure legend. The results are presented as mean values with a ± standard error of the mean (SEM). The data were analyzed using SPSS statistical software for Microsoft Windows, release 6.0 (Professional Statistic, Chicago, IL, USA). For comparison of two groups two-tailed Student t-test was used. Mann Whitney-U test was used for comparison of two groups with non-normal distribution. Values were considered significantly different when $p<0.05$.

Animal experimentation

Female C57BL/6 mice, 6 weeks of age, were purchased from Envigo (Barcelona, Spain). All mice were housed in pathogen-free, ventilated cages in the animal facility at the University of Murcia in accordance with the Spanish legislation and directives of the European Community. All animal procedures were approved by the Ethics Committee of the University of Murcia and the Direccion General de Ganaderia y Pesca, Comunidad Autonoma de Murcia (Project reference A13151101). Mice were monitored daily and sacrificed before any signs of distress. Mice were inoculated with 2 x 10^5 B16F10 cells subcutaneously or in the tail vein. The size of the subcutaneous tumors was measured three times weekly for the duration of the experiment with calipers. All tumors were analyzed using the IVIS Imaging System (Caliper Life Sciences, Hopkinton, MA, USA).

Human samples and immunohistochemistry

Melanoma patient samples were obtained from surgical resections of patients diagnosed with melanoma at Hospital Clínico San Carlos (Madrid, Spain).

Staining was conducted on 5 µm sections. Slides were deparaffinized by incubation at 60˚C for 10 min and then incubated with PT-Link (Dako, Agilent) for 20 min at 95˚C at pH 6.0 to detect TFEB. Slides in slide-holders were incubated with peroxidase blocking reagent (Dako, Agilent) and then with the following dilutions of antibodies: anti-TFEB (1:50) overnight at 4˚C. Slides were incubated for 20 min with the appropriate HRP-conjugated anti-Ig (EnVision, Dako, Agilent). Sections were then visualized with the HRP Magenta (Dako, Agilent), and counterstained for 5 min with Harrys' Haematoxylin (Sigma Aldrich, Merck). Photographs were taken with a Zeis microscope with a 20x objective.

Patient Characteristics	**N (%)**
Gender	
Male	1 (33.3%)
Female	2 (66.6%)
Age, n(%)	
< 60	1 (33.3%)
> 60	2 (66.6%)
Breslow (median, mm)	2.7
Clark level, n(%)	
I	0 (0%)

II	0 (0%)
III	0 (0%)
IV	3 (100%)
Histologic type, n (%)	
NM	2 (66.6%)
NA	1 (33.3%)
Ulceration, n (%)	
Yes	1 (33.3%)
No	0 (0%)
NA	2 (66.6%)
Metastasis development	
Yes	2 (66.6%)
No	1 (33.3%)

RNA-seq

Cells were allowed to reach 80% confluency in a 6-well plate before total RNA was extracted using RNeasy kit (QIAGEN #74106) as per manufacturer protocol. 500 ng total RNA were used for library preparation using QuantSeq Forward kit (LEXOGEN #015.96) according to the manufacturer's protocol before sequencing by the Wellcome Trust genomic service, Oxford.

ChIP-seq

The ChIP protocol used here was the same as that previously used for HA-MITF ChIP seq. Cells were grown in 15 cm^2 dishes to reach 70-80% confluency with each replicate making up to 30 dishes. Cells were washed with 1x PBS and trypsinised with 4 mL of trypsin before being collected with 20 mL of warm medium into a 50 mL Falcon placed on ice. Cells were then centrifuged at 800 g for 4 min at 4 ºC. The medium was aspirated and the cell pellet resuspended in 1 mL of ice-cold 1x PBS, to which 35 mL of ice-cold 1x PBS 0.4% PFA was added for crosslinking proteins to the DNA. The Falcon tubes were then kept on a roller for 10 min at room temperature before the crosslinking reaction was stopped by adding 4 mL of 2 M Glycine (0.2 M final concentration) to quench the PFA for a further 10 min at room temperature on the roller. Tubes were then centrifuged at 1500 g for 10 min at 4 ºC and the supernatant removed. At this stage, the cell pellets were frozen at -80 °C. Then 1 ml of fresh ChIP lysis buffer (50 mM Tris-HCl (pH 8.0), 10 mM EDTA, 10 mM sodium butyrate, 1% SDS, 4×PIC (Roche; Cat#05056489001)) was added to the pellets. PIC and PhosStop were added to the buffer just immediately prior to use. Replicate lysates were pooled and broken down by using a 25 G needle and a 20 ml syringe, and aliquoted into Covaris 1 ml vials that were sonicated in a S220 sonicator (Covaris) for 15 min at 160 W, with 5% duty cycle and 200 cycles per burst. Sonicated DNA was then transferred from the Covaris vessel to a 1.5 ml Eppendorf tube and centrifuged at 13,000 g for 10 min at 4 ºC. The cleared supernatant was then transferred to a fresh 1.5 ml Eppendorf tube stored at -80°C after two 10 µl aliquots were transferred to a new tube. One aliquot was kept as a 1% input control and frozen at -80 °C. The second aliquot was reverse-crosslinked overnight to

check for DNA fragment size by running the purified sample on a 2% agarose gel to confirm successful sonication and a desired size of fragment size of 200-400 bp. Once correct fragmentation had been achieved, DNA samples were thawed at 4 ºC and diluted with ChIP dilution buffer to 9 ml in a 50 ml Falcon tube. Next, 120 µg of HA antibody (Roche) was used per 30 dishes and the 50 ml Falcons left rotating and incubating overnight in the cold room at 4 ºC. In parallel, using an Eppendorf magnetic rack, 600 µl of Protein G Dynabeads were washed, resuspended and ultimately blocked overnight in a 1.5 mL tube with ChIP dilution buffer containing 0.5 mg/ml of BSA (Sigma) at 4ºC in a rotator in the cold room. For the pulldown, blocked Dynabeads were added to the sample and rotated for 60 min at 4ºC in the cold room, before being centrifuged for 10 min at 1500 g and 4 ºC. The supernatant was removed and all further washing steps carried out with the use of a microcentrifuge tube magnetic rack in the 4 ºC cold room, with the beads transferred to a fresh new tube after each washing step. Beads were resuspended in 1 ml of ChIP low salt wash buffer and transferred to a new 1.5 ml microcentrifuge tube, washed again and resuspended in another 1 ml of ChIP low salt wash buffer before being placed in a new tube. Beads were then washed twice more with ChIP low salt wash buffer followed by 2x washes with ChIP high salt wash buffer, then 2x washes with LiCl wash buffer. Finally, ChIP samples were simultaneously eluted with freshly made microwaved elution buffer and reverse cross-linked overnight in a Eppendorf shaker set at 55 ºC and 600 rpm, to release the proteins from the beads and the DNA fragments from the proteins. ChIP DNA was recovered using a PCR purification kit according to the manufacturer's instructions, with the caveat that the first elution step was made with 30 µl for ChIP-seq library preparation and the second elution with 120 µl was kept for ChIP-qPCR. ChIP and Input samples were tested on Qubit and Bioanalyzer to confirm amount and integrity of the samples before being sent for sequencing

2.4.11 – ChIP Quantitative PCR

To quantify and analyze the enrichment of DNA in the ChIP samples versus the input samples the ChIP-qPCR reaction was carried out according to the Brilliant III Ultra-Fast SYBR Green QPCR Master Mix protocol in a Rotor-Gene 6000 or Rotor-Gene Q real-time thermal cycler. A 15 µl reaction was made up of 7.5 µl of SYBR Green Mix, a 2 µl mix of forward and reverse primers from a working stock of 10 µM and 5.5 µl of DNA template. The ChIP-qPCR reaction was run on a Rotor-Gene 6000 or Rotor-Gene Q real-time thermal cycler according to the manufacturer's instructions. The resulting ChIP-qPCR data was analyzed by using the percent input method to normalize the data, whereby the signal from the ChIP is divided from the signal of the input sample which represents the amount of chromatin that was used in the ChIP. For example, if the starting input fraction is 1%, then a diluting factor (DF) of 100 which corresponds to 6.644 cycles (log2 of 100) is subtracted from the input Ct values.

Bioinformatics analyses

B16 RNA-seq and TFE3 ChIP-seq libraries were sequenced on an Illumina NovaSeq 6000. TFEB ChIP-seq libraries were sequenced on an Illumina HiSeq 4000. 501mel RNA seq were sequenced on NextSeq

550. Base calling and demultiplexing were carried out by the Oxford Genomic Centre Service, University of Oxford.

Fastq reads for each sample were sequenced across multiple flow cells (except B16 RNA-seq libraries which were sequenced on a single flow cell) and were stitched on UNIX and quality controlled using fastqc (v.0.11.9).

ChIP-seq samples were adaptors and 2 colour-trimmed as paired-end reads while RNA-seq were also trimmed of poly-A as single-end reads using trim_galore (v.0.6.5; running python-base v.3.6.10, cutadapt v.2.10, java v.17.0.1, fastqc v.0.11.9 and pigz v.2.4) [116].

B16 trimmed reads were mapped to the *Mus musculus* reference genome (mm39) with STAR (v.2.7.8a) [117]. 501mel trimmed reads were mapped to the Human reference genome (hg38) with STAR (version 2.7.8a). RNA-seq normalisation and differential gene expression analyses were performed as previously described [13,21,124] using edgeR glmQLFTest. GSEA analyses were performed using pre-ranked lists derived from edgeR glmQLFTest $-\log_{10}$(P-value)/sign(logFC) using GSEA (v.4.3.2) against MSigDB v2022.1. Dot blot of GSEA analyses were generated using pre-ranked list above using the Bioconductor packages clusterProfiler (v4.6.2), DOSE (v3.24.2). Genesets from MSigDB were imported using the package msigdbr (v7.5.1).

TFEB and TFE3 ChIP-seq trimmed fastq files were mapped using STAR (v.2.5.1b or v.2.7.8a, respectively) [117] against the human hg38 index. Peak calling, *de novo* motif identification, genome ontology analyses were performed using Homer as previously described [69,124]. Normalised bigwig of aligned reads were generated using Homer for visualisation on the UCSC genome browser as MultiWig hubs. The peaks calling parameter were: FDR rate threshold = 0.001, Fold over input = 4.00, Poisson p-value over input = 1.00e-04, Fold over local region = 4.00, Poisson p-value over local region = 1.00e-04 and variable parameters (modelled according to each dataset as these are sequencing depth dependent), FDR effective poisson threshold and FDR tag threshold

Data visualisation

Overlapping peaks were visualised using a R package VennDiagram (v.1.7.3). Genome ontology, box and jitter plots, volcano plots and peak correlation plots were generated using an R package ggplot2 (v.3.4.4). Heatmaps and hierarchical clustering of normalised gene expression were performed using an R package pheatmap (v.1.0.12). Tag density of ChIP-seq datasets were visualised using the java package TreeView (v.1.1.6) [120].

GSEA dot plots were generated using the Bioconductor package enrichplot (v.1.18.4) using the cut-off adjusted-p-value of 0.05 (Benjamini-Hochberg procedure).

Moving average plots were generated using TCGA $\log_2$ of RSEM transcript abundance quantification using 20 samples window. Spearman's ρ computation and correlation tests were performed using R cor.test function.

Ethics Statement

This study using human melanoma tissue was reviewed and approved by the Institutional Review Board (IRB) of Clínico San Carlos Hospital on June 25, 2021 (C.I. 21/498-E). All patients gave written informed consent for the use of their biological samples for research purposes. Fundamental ethical principles and rights promoted by Spain (LOPD 15/1999) and the European Union (2000/C364/01) were followed. Patient data were processed according to the Declaration of Helsinki (last revision 2013) and Spanish National Biomedical Research Law (14/2007, July 3).

All animal procedures were approved by the Ethics Committee of the University of Murcia and the Direccion General de Ganaderia y Pesca, Comunidad Autonoma de Murcia (Project reference A13151101). Mice were monitored daily and sacrificed before any signs of distress.

Acknowledgements

We thank Pati Faria-Shayler for technical support. This work was funded by the Ludwig Institute for Cancer Research (CRG, PL, SA, LM), The National Institutes of Health R01 CA268597-01 (CRG, PL) and PO1 CA128814-06A1 (YV-G), GABBA, University of Porto (DD) and Fundacao de Amparo a Pesquisa do Estado de Sao Paulo (FAPESP) (EO), La Caixa (LM), China Scholarship Council (LL). This work was also supported by a project funded by the Fundación Robles Chillida (Caravaca, Murcia) (L.S-d-C) and the Fundación Séneca, Región de Murcia (FS-RM) (20809/PI/18) to (JNR-L). L.S-d-C was contracted by the Ramon y Cajal Programme (RYC-2016-20036) and RMD has a fellowship from Fundación Séneca, Región de Murcia (Spain) (21407/FPI/20). Additional support was provided by the Agencia Estatal de Investigación: MCIN/AEI/10.13039/501100011033 PID2023-151128OB-100 and PID2019-10487RB-100 (CG-J) and PID2021-127645OA-100 (ACC), and by Comunidad de Madrid: PEJ-2021-AI/BMD-22973, PEJ-2021-TL/BMD-21515 and PRECICOLON-CM, P2022/BMD-7212 (CG-J).

Data availability

All sequencing datasets have been deposited at the Gene Expression Omnibus (GEO) with the following accession numbers:

RNA-seq from MITF, TFEB and TFE3 B16 KO cell lines: GSE270594

RNA-seq from 501mel cell lines: GSE277250

TFEB ChIP-seq: GSE270585

TFE3 ChIP-seq: GSE270590

shMITF RNA-seq: GSE255256

RNA-seq from inducible CTNNB1 in IGR37 cells: GSE136803

Author contributions

C.R.G. and P.L conceived the project and designed and interpreted experiments. D.D., E.O., S.A, L.M, L.L. R.M.D., Y.V-G. and P.L. performed experiments, A.C-C. and J.M.G-M undertook IHC analysis, J.C. and P.L. provided bioinformatic analysis P.L., LS-d-C, C.G-J., J.N.R-L., SSM-E and C.R.G. provided resources and supervision. C.R.G., P.L. C. G-J. and LS-d-C wrote the manuscript.

Declaration of Interests
The authors declare no competing interests

Supplemental information

Supplemental Figure S1: Immunofluorescence and Western blotting showing subcellular localization of TFEB and TFE3 in melanoma cells

Supplemental Figure S2: ChIP-seq of HA-TFEB and HA-TFE3

Supplemental Figure S3: Differential regulation of genes in parental or TFEB/TFE3 KO 501mel after Torin treatment.

Supplemental Figure S4: MITF/TFE factors control proliferation.

Supplemental Figure S5: MITF factor ChIP at the *TFEB*, *TFE3* and example genes.

Supplemental Table S1: DEGs in 501mel KO cells.

Supplemental Table S2: DEGs in B16 KO cells.

Supplemental Table S3: HALLMARK Interferon Alpha Response genes bound by MITF family members.

References

1. Lambert, S.A., Jolma, A., Campitelli, L.F., Das, P.K., Yin, Y., Albu, M., Chen, X., Taipale, J., Hughes, T.R., and Weirauch, M.T. (2018). The Human Transcription Factors. Cell *172*, 650-665. 10.1016/j.cell.2018.01.029.
2. Yuan, S., Norgard, R.J., and Stanger, B.Z. (2019). Cellular Plasticity in Cancer. Cancer Discov *9*, 837-851. 10.1158/2159-8290.CD-19-0015.
3. Quintanal-Villalonga, A., Chan, J.M., Yu, H.A., Pe'er, D., Sawyers, C.L., Sen, T., and Rudin, C.M. (2020). Lineage plasticity in cancer: a shared pathway of therapeutic resistance. Nat Rev Clin Oncol *17*, 360-371. 10.1038/s41571-020-0340-z.
4. Lambert, A.W., Zhang, Y., and Weinberg, R.A. (2024). Cell-intrinsic and microenvironmental determinants of metastatic colonization. Nat Cell Biol *26*, 687-697. 10.1038/s41556-024-01409-8.
5. García-Jiménez, C., and Goding, C.R. (2019). Starvation and Pseudo-Starvation as Drivers of Cancer Metastasis through Translation Reprogramming. Cell Metab *29*, 258-267.
6. Falletta, P., Goding, C.R., and Vivas-Garcia, Y. (2022). Connecting Metabolic Rewiring With Phenotype Switching in Melanoma. Front Cell Dev Biol *10*, 930250. 10.3389/fcell.2022.930250.
7. Rambow, F., Marine, J.C., and Goding, C.R. (2019). Melanoma plasticity and phenotypic diversity: therapeutic barriers and opportunities Genes Dev *33*, 1295-1318.
8. Garraway, L.A., Widlund, H.R., Rubin, M.A., Getz, G., Berger, A.J., Ramaswamy, S., Beroukhim, R., Milner, D.A., Granter, S.R., Du, J., et al. (2005). Integrative genomic analyses identify MITF as a lineage survival oncogene amplified in malignant melanoma. Nature *436*, 117-122.
9. Goding, C.R., and Arnheiter, H. (2019). MITF - The first 25 years. Genes Dev *33*, 983-1007. doi: 10.1101/gad.324657.119.
10. Falletta, P., Sanchez-del-Campo, L., Chauhan, J., Effern, M., Kenyon, A., Kershaw, C.J., Siddaway, R., Lisle, R., Freter, R., Daniels, M., et al. (2017). Translation reprogramming is an evolutionarily conserved driver of phenotypic plasticity and therapeutic resistance in melanoma. Genes Dev *31*, 18-33.
11. Ferguson, J., Smith, M., Zudaire, I., Wellbrock, C., and Arozarena, I. (2017). Glucose availability controls ATF4-mediated MITF suppression to drive melanoma cell growth. Oncotarget *8*, 32946-32959. 10.18632/oncotarget.16514.
12. Cheli, Y., Giuliano, S., Fenouille, N., Allegra, M., Hofman, V., Hofman, P., Bahadoran, P., Lacour, J.P., Tartare-Deckert, S., Bertolotto, C., and Ballotti, R. (2012). Hypoxia and MITF control metastatic behaviour in mouse and human melanoma cells. Oncogene *31*, 2461-2470. 10.1038/onc.2011.425.
13. Louphrasitthiphol, P., Ledaki, I., Chauhan, J., Falletta, P., Siddaway, R., Buffa, F.M., Mole, D.R., Soga, T., and Goding, C.R. (2019). MITF controls the TCA cycle to modulate the melanoma hypoxia response. Pigment Cell Melanoma Res *32*, 792-808. 10.1111/pcmr.12802.
14. McGill, G.G., Horstmann, M., Widlund, H.R., Du, J., Motyckova, G., Nishimura, E.K., Lin, Y.L., Ramaswamy, S., Avery, W., Ding, H.F., et al. (2002). Bcl2 regulation by the melanocyte master regulator mitf modulates lineage survival and melanoma cell viability. Cell *109*, 707-718.
15. Widlund, H.R., Horstmann, M.A., Price, E.R., Cui, J., Lessnick, S.L., Wu, M., He, X., and Fisher, D.E. (2002). Beta-catenin-induced melanoma growth requires the downstream target Microphthalmia-associated transcription factor. J Cell Biol *158*, 1079-1087. 10.1083/jcb.200202049.
16. Du, J., Widlund, H.R., Horstmann, M.A., Ramaswamy, S., Ross, K., Huber, W.E., Nishimura, E.K., Golub, T.R., and Fisher, D.E. (2004). Critical role of CDK2 for melanoma growth linked to its melanocyte-specific transcriptional regulation by MITF. Cancer Cell *6*, 565-576.

17. Loercher, A.E., Tank, E.M., Delston, R.B., and Harbour, J.W. (2005). MITF links differentiation with cell cycle arrest in melanocytes by transcriptional activation of INK4A. J Cell Biol *168*, 35-40. Epub 2004 Dec 2028.
18. Carreira, S., Goodall, J., Aksan, I., La Rocca, S.A., Galibert, M.D., Denat, L., Larue, L., and Goding, C.R. (2005). Mitf cooperates with Rb1 and activates p21Cip1 expression to regulate cell cycle progression. Nature *433*, 764-769. 10.1038/nature03269.
19. Haq, R., Shoag, J., Andreu-Perez, P., Yokoyama, S., Edelman, H., Rowe, G.C., Frederick, D.T., Hurley, A.D., Nellore, A., Kung, A.L., et al. (2013). Oncogenic BRAF regulates oxidative metabolism via PGC1alpha and MITF. Cancer cell *23*, 302-315. 10.1016/j.ccr.2013.02.003.
20. Vazquez, F., Lim, J.H., Chim, H., Bhalla, K., Girnun, G., Pierce, K., Clish, C.B., Granter, S.R., Widlund, H.R., Spiegelman, B.M., and Puigserver, P. (2013). PGC1alpha expression defines a subset of human melanoma tumors with increased mitochondrial capacity and resistance to oxidative stress. Cancer Cell *23*, 287-301. 10.1016/j.ccr.2012.11.020.
21. Vivas-Garcia, Y., Falletta, P., Liebing, J., Louphrasitthiphol, P., Feng, Y., Chauhan, J., Scott, D.A., Glodde, N., Chocarro-Calvo, A., Bonham, S., et al. (2020). Lineage-Restricted Regulation of SCD and Fatty Acid Saturation by MITF Controls Melanoma Phenotypic Plasticity. Mol Cell *77*, 120-139. 10.1016/j.molcel.2019.10.014.
22. Binet, R., Lambert, J.P., Tomkova, M., Tischfield, S., Baggiolini, A., Picaud, S., Sarkar, S., Louphrasitthiphol, P., Dias, D., Carreira, S., et al. (2024). DNA damage remodels the MITF interactome to increase melanoma genomic instability. Genes Dev *38*, 70-94. 10.1101/gad.350740.123.
23. Strub, T., Giuliano, S., Ye, T., Bonet, C., Keime, C., Kobi, D., Le Gras, S., Cormont, M., Ballotti, R., Bertolotto, C., and Davidson, I. (2011). Essential role of microphthalmia transcription factor for DNA replication, mitosis and genomic stability in melanoma. Oncogene *30*, 2319-2332. onc2010612 [pii]10.1038/onc.2010.612.
24. Giuliano, S., Cheli, Y., Ohanna, M., Bonet, C., Beuret, L., Bille, K., Loubat, A., Hofman, V., Hofman, P., Ponzio, G., et al. (2010). Microphthalmia-associated transcription factor controls the DNA damage response and a lineage-specific senescence program in melanomas. Cancer Res *70*, 3813-3822. 0008-5472.CAN-09-2913 [pii]10.1158/0008-5472.CAN-09-2913.
25. Carreira, S., Goodall, J., Denat, L., Rodriguez, M., Nuciforo, P., Hoek, K.S., Testori, A., Larue, L., and Goding, C.R. (2006). Mitf regulation of Dia1 controls melanoma proliferation and invasiveness. Genes Dev *20*, 3426-3439. 10.1101/gad.406406.
26. Goodall, J., Carreira, S., Denat, L., Kobi, D., Davidson, I., Nuciforo, P., Sturm, R.A., Larue, L., and Goding, C.R. (2008). Brn-2 represses microphthalmia-associated transcription factor expression and marks a distinct subpopulation of microphthalmia-associated transcription factor-negative melanoma cells. Cancer Res *68*, 7788-7794. 10.1158/0008-5472.CAN-08-1053.
27. Cheli, Y., Giuliano, S., Botton, T., Rocchi, S., Hofman, V., Hofman, P., Bahadoran, P., Bertolotto, C., and Ballotti, R. (2011). Mitf is the key molecular switch between mouse or human melanoma initiating cells and their differentiated progeny. Oncogene *30*, 2307-2318. 10.1038/onc.2010.598.
28. Konieczkowski, D.J., Johannessen, C.M., Abudayyeh, O., Kim, J.W., Cooper, Z.A., Piris, A., Frederick, D.T., Barzily-Rokni, M., Straussman, R., Haq, R., et al. (2014). A melanoma cell state distinction influences sensitivity to MAPK pathway inhibitors. Cancer Discov*4*, 816-827. 10.1158/2159-8290.CD-13-0424.
29. Muller, J., Krijgsman, O., Tsoi, J., Robert, L., Hugo, W., Song, C., Kong, X., Possik, P.A., Cornelissen-Steijger, P.D., Foppen, M.H., et al. (2014). Low MITF/AXL ratio predicts early resistance to multiple targeted drugs in melanoma. Nat Commun *5*, 5712. 10.1038/ncomms6712.
30. Rambow, F., Job, B., Petit, V., Gesbert, F., Delmas, V., Seberg, H., Meurice, G., Van Otterloo, E., Dessen, P., Robert, C., et al. (2015). New Functional Signatures for Understanding Melanoma Biology from Tumor Cell Lineage-Specific Analysis. Cell Reports *13*, 840-853. 10.1016/j.celrep.2015.09.037.

31. Karras, P., Bordeu, I., Pozniak, J., Nowosad, A., Pazzi, C., Van Raemdonck, N., Landeloos, E., Van Herck, Y., Pedri, D., Bervoets, G., et al. (2022). A cellular hierarchy in melanoma uncouples growth and metastasis. Nature *610*, 190-198. 10.1038/s41586-022-05242-7.
32. Hoek, K., and Goding, C.R. (2010). Cancer stem cells versus phenotype switching in melanoma. Pigment Cell Melanoma Res. *23*, 746-759.
33. Raben, N., and Puertollano, R. (2016). TFEB and TFE3: Linking Lysosomes to Cellular Adaptation to Stress. Annu Rev Cell Dev Biol *32*, 255-278. 10.1146/annurev-cellbio-111315-125407.
34. La Spina, M., Contreras, P.S., Rissone, A., Meena, N.K., Jeong, E., and Martina, J.A. (2020). MiT/TFE Family of Transcription Factors: An Evolutionary Perspective. Front Cell Dev Biol *8*, 609683. 10.3389/fcell.2020.609683.
35. Sardiello, M., Palmieri, M., di Ronza, A., Medina, D.L., Valenza, M., Gennarino, V.A., Di Malta, C., Donaudy, F., Embrione, V., Polishchuk, R.S., et al. (2009). A gene network regulating lysosomal biogenesis and function. Science *325*, 473-477. 1174447 [pii] 10.1126/science.1174447.
36. Settembre, C., Di Malta, C., Polito, V.A., Garcia Arencibia, M., Vetrini, F., Erdin, S., Erdin, S.U., Huynh, T., Medina, D., Colella, P., et al. (2011). TFEB links autophagy to lysosomal biogenesis. Science *332*, 1429-1433. 10.1126/science.1204592.
37. Martina, J.A., Diab, H.I., Lishu, L., Jeong, A.L., Patange, S., Raben, N., and Puertollano, R. (2014). The Nutrient-Responsive Transcription Factor TFE3 Promotes Autophagy, Lysosomal Biogenesis, and Clearance of Cellular Debris. Science Signaling *7*, ra9. 10.1126/scisignal.2004754.
38. Martina, J.A.A., Diab, H.I., Brady, O.A., and Puertollano, R. (2016). TFEB and TFE3 are novel components of the integrated stress response. EMBO J *35*, 479-495. 10.15252/embj.201593428.
39. Avelar, A.R., Gupta, R., Carvette, G., da Veiga Leprevost, F., Jasti, M., Colina, J., Teitel, J., Nesvizhskii, A.I., O'Connor, C.M., Hatzoglou, M., et al. (2024). Integrated stress response plasticity governs normal cell adaptation to chronic stress via the PP2A-TFE3-ATF4 pathway. Cell Death Differ. 10.1038/s41418-024-01378-3.
40. Pasquier, A., Pastore, N., D'Orsi, L., Colonna, R., Esposito, A., Maffia, V., De Cegli, R., Mutarelli, M., Ambrosio, S., Tufano, G., et al. (2023). TFEB and TFE3 control glucose homeostasis by regulating insulin gene expression. EMBO J *42*, e113928. 10.15252/embj.2023113928.
41. Pastore, N., Brady, O.A., Diab, H.I., Martina, J.A., Sun, L., Huynh, T., Lim, J.A., Zare, H., Raben, N., Ballabio, A., and Puertollano, R. (2016). TFEB and TFE3 cooperate in the regulation of the innate immune response in activated macrophages. Autophagy *12*, 1240-1258. 10.1080/15548627.2016.1179405.
42. El-Houjeiri, L., Possik, E., Vijayaraghavan, T., Paquette, M., Martina, J.A., Kazan, J.M., Ma, E.H., Jones, R., Blanchette, P., Puertollano, R., and Pause, A. (2019). The Transcription Factors TFEB and TFE3 Link the FLCN-AMPK Signaling Axis to Innate Immune Response and Pathogen Resistance. Cell Reports *26*, 3613-3628 e3616. 10.1016/j.celrep.2019.02.102.
43. Mansueto, G., Armani, A., Viscomi, C., D'Orsi, L., De Cegli, R., Polishchuk, E.V., Lamperti, C., Di Meo, I., Romanello, V., Marchet, S., et al. (2016). Transcription Factor EB Controls Metabolic Flexibility during Exercise. Cell Metab *25*, 182-196. 10.1016/j.cmet.2016.11.003.
44. Garcia-Prat, L., Kaufmann, K.B., Schneiter, F., Voisin, V., Murison, A., Chen, J., Chan-Seng-Yue, M., Gan, O.I., McLeod, J.L., Smith, S.A., et al. (2021). TFEB-mediated endolysosomal activity controls human hematopoietic stem cell fate. Cell Stem Cell *28*, 1838-1850 e1810. 10.1016/j.stem.2021.07.003.
45. Young, N.P., Kamireddy, A., Van Nostrand, J.L., Eichner, L.J., Shokhirev, M.N., Dayn, Y., and Shaw, R.J. (2016). AMPK governs lineage specification through Tfeb-dependent regulation of lysosomes. Genes Dev *30*, 535-552. 10.1101/gad.274142.115.
46. Roczniak-Ferguson, A., Petit, C.S., Froehlich, F., Qian, S., Ky, J., Angarola, B., Walther, T.C., and Ferguson, S.M. (2012). The transcription factor TFEB links mTORC1 signaling to transcriptional control of lysosome homeostasis. Science Signal*5*, ra42. 10.1126/scisignal.2002790.

47. Puertollano, R., Ferguson, S.M., Brugarolas, J., and Ballabio, A. (2018). The complex relationship between TFEB transcription factor phosphorylation and subcellular localization. EMBO J *37*, E98804. 10.15252/embj.201798804.
48. Martina, J.A., and Puertollano, R. (2013). Rag GTPases mediate amino acid-dependent recruitment of TFEB and MITF to lysosomes. J Cell Biol *200*, 475-491. 10.1083/jcb.201209135.
49. Napolitano, G., Di Malta, C., Esposito, A., de Araujo, M.E.G., Pece, S., Bertalot, G., Matarese, M., Benedetti, V., Zampelli, A., Stasyk, T., et al. (2020). A substrate-specific mTORC1 pathway underlies Birt-Hogg-Dube syndrome. Nature *585*, 597-602. 10.1038/s41586-020-2444-0.
50. Nardone, C., Palanski, B.A., Scott, D.C., Timms, R.T., Barber, K.W., Gu, X., Mao, A., Leng, Y., Watson, E.V., Schulman, B.A., et al. (2023). A central role for regulated protein stability in the control of TFE3 and MITF by nutrients. Mol Cell *83*, 57-73 e59. 10.1016/j.molcel.2022.12.013.
51. Medina, D.L., Di Paola, S., Peluso, I., Armani, A., De Stefani, D., Venditti, R., Montefusco, S., Scotto-Rosato, A., Prezioso, C., Forrester, A., et al. (2015). Lysosomal calcium signalling regulates autophagy through calcineurin and TFEB. Nat Cell Biology *17*, 288-299. 10.1038/ncb3114.
52. Martina, J.A., and Puertollano, R. (2018). Protein phosphatase 2A stimulates activation of TFEB and TFE3 transcription factors in response to oxidative stress. J Biol Chem *293*, 12525-12534. 10.1074/jbc.RA118.003471.
53. Perera, R.M., Stoykova, S., Nicolay, B.N., Ross, K.N., Fitamant, J., Boukhali, M., Lengrand, J., Deshpande, V., Selig, M.K., Ferrone, C.R., et al. (2015). Transcriptional control of autophagy-lysosome function drives pancreatic cancer metabolism. Nature *524*, 361-365. 10.1038/nature14587.
54. Wu, X., and Eisenman, R.N. (2021). MYC and TFEB Control DNA Methylation and Differentiation in AML. Blood Cancer Discov *2*, 116-118. 10.1158/2643-3230.BCD-20-0230.
55. Zoncu, R., and Perera, R.M. (2023). Emerging roles of the MiT/TFE factors in cancer. Trends Cancer *9*, 817-827. 10.1016/j.trecan.2023.06.005.
56. Ariano, C., Costanza, F., Akman, M., Riganti, C., Cora, D., Casanova, E., Astanina, E., Comunanza, V., Bussolino, F., and Doronzo, G. (2023). TFEB inhibition induces melanoma shut-down by blocking the cell cycle and rewiring metabolism. Cell Death Disease *14*, 314. 10.1038/s41419-023-05828-7.
57. Ben-Sahra, I., and Manning, B.D. (2017). mTORC1 signaling and the metabolic control of cell growth. Curr Op Cell Biol *45*, 72-82. 10.1016/j.ceb.2017.02.012.
58. Cui, Z., Napolitano, G., de Araujo, M.E.G., Esposito, A., Monfregola, J., Huber, L.A., Ballabio, A., and Hurley, J.H. (2023). Structure of the lysosomal mTORC1-TFEB-Rag-Ragulator megacomplex. Nature *614*, 572-579. 10.1038/s41586-022-05652-7.
59. Jansen, R.M., Peruzzo, R., Fromm, S.A., Yokom, A.L., Zoncu, R., and Hurley, J.H. (2022). Structural basis for FLCN RagC GAP activation in MiT-TFE substrate-selective mTORC1 regulation. Sci Adv *8*, eadd2926. 10.1126/sciadv.add2926.
60. Lawrence, R.E., Fromm, S.A., Fu, Y., Yokom, A.L., Kim, D.J., Thelen, A.M., Young, L.N., Lim, C.Y., Samelson, A.J., Hurley, J.H., and Zoncu, R. (2019). Structural mechanism of a Rag GTPase activation checkpoint by the lysosomal folliculin complex. Science *366*, 971-977. 10.1126/science.aax0364.
61. Tsoi, J., Robert, L., Paraiso, K., Galvan, C., Sheu, K.M., Lay, J., Wong, D.J.L., Atefi, M., Shirazi, R., Wang, X., et al. (2018). Multi-stage Differentiation Defines Melanoma Subtypes with Differential Vulnerability to Drug-Induced Iron-Dependent Oxidative Stress. Cancer Cell *33*, 890-904 e895. 10.1016/j.ccell.2018.03.017.
62. Louphrasitthiphol, P., Siddaway, R., Loffreda, A., Pogenberg, V., Friedrichsen, H., Schepsky, A., Faria-Shayler, P., Zeng, Z., Lu, M., Strub, T., et al. (2020). Tuning transcription factor availability through acetylation-mediated genomic redistribution. Mol Cell *79*, 472–487.
63. Schepsky, A., Bruser, K., Gunnarsson, G.J., Goodall, J., Hallsson, J.H., Goding, C.R., Steingrimsson, E., and Hecht, A. (2006). The microphthalmia-associated transcription factor

Mitf interacts with beta-catenin to determine target gene expression. Mol Cell Biol. *26*, 8914-8927.
64. Dorsky, R.I., Raible, D.W., and Moon, R.T. (2000). Direct regulation of *nacre*, a zebrafish MITF homolog required for pigment cell formation, by the Wnt pathway. Genes Dev. *14*, 158-162.
65. Moller, K., Sigurbjornsdottir, S., Arnthorsson, A.O., Pogenberg, V., Dilshat, R., Fock, V., Brynjolfsdottir, S.H., Bindesboll, C., Bessadottir, M., Ogmundsdottir, H.M., et al. (2019). MITF has a central role in regulating starvation-induced autophagy in melanoma. Scientific Reports *9*, 1055. 10.1038/s41598-018-37522-6.
66. Dickson, B.C., Brooks, J.S., Pasha, T.L., and Zhang, P.J. (2011). TFE3 expression in tumors of the microphthalmia-associated transcription factor (MiTF) family. Int J Surg Pathol *19*, 26-30. 10.1177/1066896909352861.
67. Li, L., Friedrichsen, H.J., Andrews, S., Picaud, S., Volpon, L., Ngeow, K., Berridge, G., Fischer, R., Borden, K.L.B., Filippakopoulos, P., and Goding, C.R. (2018). A TFEB nuclear export signal integrates amino acid supply and glucose availability. Nat Commun *9*, 2685. 10.1038/s41467-018-04849-7.
68. Settembre, C., Zoncu, R., Medina, D.L., Vetrini, F., Erdin, S., Erdin, S., Huynh, T., Ferron, M., Karsenty, G., Vellard, M.C., et al. (2012). A lysosome-to-nucleus signalling mechanism senses and regulates the lysosome via mTOR and TFEB. EMBO J *31*, 1095-1108. 10.1038/emboj.2012.32.
69. Louphrasitthiphol, P., Loffreda, A., Pogenberg, V., Picaud, S., Schepsky, A., Friedrichsen, H., Zeng, Z., Lashgari, A., Thomas, B., Patton, E.E., et al. (2023). Acetylation reprograms MITF target selectivity and residence time. Nat Commun *14*, 6051. 10.1038/s41467-023-41793-7.
70. Napolitano, G., Esposito, A., Choi, H., Matarese, M., Benedetti, V., Di Malta, C., Monfregola, J., Medina, D.L., Lippincott-Schwartz, J., and Ballabio, A. (2018). mTOR-dependent phosphorylation controls TFEB nuclear export. Nat Commun *9*, 3312. 10.1038/s41467-018-05862-6.
71. Aksan, I., and Goding, C.R. (1998). Targeting the microphthalmia basic helix-loop-helix-leucine zipper transcription factor to a subset of E-box elements in vitro and in vivo. Mol Cell Biol *18*, 6930-6938.
72. Lickwar, C.R., Mueller, F., Hanlon, S.E., McNally, J.G., and Lieb, J.D. (2012). Genome-wide protein-DNA binding dynamics suggest a molecular clutch for transcription factor function. Nature *484*, 251-255. nature10985 [pii] 10.1038/nature10985.
73. Seoane, M., Buhs, S., Iglesias, P., Strauss, J., Puller, A.C., Muller, J., Gerull, H., Feldhaus, S., Alawi, M., Brandner, J.M., et al. (2019). Lineage-specific control of TFIIH by MITF determines transcriptional homeostasis and DNA repair. Oncogene. 10.1038/s41388-018-0661-x.
74. Beuret, L., Ohanna, M., Strub, T., Allegra, M., Davidson, I., Bertolotto, C., and Ballotti, R. (2011). BRCA1 is a new MITF target gene. Pigment Cell Melanoma Res *24*, 725-727. 10.1111/j.1755-148X.2011.00862.x.
75. Sanchez-Del-Campo, L., Marti-Diaz, R., Montenegro, M.F., Gonzalez-Guerrero, R., Hernandez-Caselles, T., Martinez-Barba, E., Pinero-Madrona, A., Cabezas-Herrera, J., Goding, C.R., and Rodriguez-Lopez, J.N. (2021). MITF induces escape from innate immunity in melanoma. J Exp Clin Cancer Res *40*, 117. 10.1186/s13046-021-01916-8.
76. Dilshat, R., Fock, V., Kenny, C., Gerritsen, I., Lasseur, R.M.J., Travnickova, J., Eichhoff, O.M., Cerny, P., Moller, K., Sigurbjornsdottir, S., et al. (2021). MITF reprograms the extracellular matrix and focal adhesion in melanoma. eLife *10*. 10.7554/eLife.63093.
77. McGill, G.G., Haq, R., Nishimura, E.K., and Fisher, D.E. (2006). c-Met expression is regulated by Mitf in the melanocyte lineage. J Biol Chem *281*, 10365-10373.
78. Zhang, M., Di Martino, J.S., Bowman, R.L., Campbell, N.R., Baksh, S.C., Simon-Vermot, T., Kim, I.S., Haldeman, P., Mondal, C., Yong-Gonzales, V., et al. (2018). Adipocyte-Derived Lipids Mediate Melanoma Progression via FATP Proteins. Cancer Dicov *8*, 1006-1025. 10.1158/2159-8290.CD-17-1371.

79. Alicea, G.M., Rebecca, V.W., Goldman, A.R., Fane, M.E., Douglass, S.M., Behera, R., Webster, M.R., Kugel, C.H., 3rd, Ecker, B.L., Caino, M.C., et al. (2020). Changes in Aged Fibroblast Lipid Metabolism Induce Age-Dependent Melanoma Cell Resistance to Targeted Therapy via the Fatty Acid Transporter FATP2. Cancer Discov *10*, 1282-1295. 10.1158/2159-8290.CD-20-0329.
80. Chocarro-Calvo, A., Jociles-Ortego, M., García-Martinez, J.M., Louphrasitthiphol, P., Vivas-Garcia, Y., Ramírez-Sánchez, A., Chauhan, J., Fuiza, M.C., Duran, M., García-Jiménez, C., and Goding, C.R. (2024). Phenotype-specific melanoma uptake of fatty acid from human adipocytes activates AXL and CAV1-dependent β-catenin nuclear accumulation. bioRxiv *doi.org/10.1101/2024.01.21.576568*.
81. Xu, D., Dai, W., Kutzler, L., Lacko, H.A., Jefferson, L.S., Dennis, M.D., and Kimball, S.R. (2020). ATF4-Mediated Upregulation of REDD1 and Sestrin2 Suppresses mTORC1 Activity during Prolonged Leucine Deprivation. J Nutr *150*, 1022-1030. 10.1093/jn/nxz309.
82. Ye, J., Palm, W., Peng, M., King, B., Lindsten, T., Li, M.O., Koumenis, C., and Thompson, C.B. (2015). GCN2 sustains mTORC1 suppression upon amino acid deprivation by inducing Sestrin2. Genes Dev *29*, 2331-2336. 10.1101/gad.269324.115.
83. Bruning, A., Rahmeh, M., and Friese, K. (2013). Nelfinavir and bortezomib inhibit mTOR activity via ATF4-mediated sestrin-2 regulation. Mol Oncol *7*, 1012-1018. 10.1016/j.molonc.2013.07.010.
84. Wolfson, R.L., Chantranupong, L., Saxton, R.A., Shen, K., Scaria, S.M., Cantor, J.R., and Sabatini, D.M. (2016). Sestrin2 is a leucine sensor for the mTORC1 pathway. Science *351*, 43-48. 10.1126/science.aab2674.
85. Marciniak, S.J., Yun, C.Y., Oyadomari, S., Novoa, I., Zhang, Y., Jungreis, R., Nagata, K., Harding, H.P., and Ron, D. (2004). CHOP induces death by promoting protein synthesis and oxidation in the stressed endoplasmic reticulum. Genes Dev *18*, 3066-3077. 10.1101/gad.1250704.
86. Rozpedek, W., Pytel, D., Mucha, B., Leszczynska, H., Diehl, J.A., and Majsterek, I. (2016). The Role of the PERK/eIF2alpha/ATF4/CHOP Signaling Pathway in Tumor Progression During Endoplasmic Reticulum Stress. Curr Mol Med *16*, 533-544.
87. Hirata, E., Girotti, M.R., Viros, A., Hooper, S., Spencer-Dene, B., Matsuda, M., Larkin, J., Marais, R., and Sahai, E. (2015). Intravital Imaging Reveals How BRAF Inhibition Generates Drug-Tolerant Microenvironments with High Integrin beta1/FAK Signaling. Cancer Cell *27*, 574-588. 10.1016/j.ccell.2015.03.008.
88. Spoerri, L., Tonnessen-Murray, C.A., Gunasingh, G., Hill, D.S., Beaumont, K.A., Jurek, R.J., Chauhan, J., Vanwalleghem, G.C., Fane, M.E., Daignault-Mill, S.M., et al. (2024). Phenotypic melanoma heterogeneity is regulated through cell-matrix interaction-dependent changes in tumor microarchitecture. bioRxiv *doi.org/10.1101/2020.06.09.141747*.
89. Polara, R., Ganesan, R., Pitson, S.M., and Robinson, N. (2024). Cell autonomous functions of CD47 in regulating cellular plasticity and metabolic plasticity. Cell Death Differ *31*, 1255-1266. 10.1038/s41418-024-01347-w.
90. Hodgkinson, C.A., Moore, K.J., Nakayama, A., Steingrimsson, E., Copeland, N.G., Jenkins, N.A., and Arnheiter, H. (1993). Mutations at the mouse *microphthalmia* locus are associated with defects in a gene encoding a novel basic-helix-loop-helix-zipper protein. Cell *74*, 395-404.
91. Ngeow, K.C., Friedrichsen, H.J., Li, L., Zeng, Z., Andrews, S., Volpon, L., Brunsdon, H., Berridge, G., Picaud, S., Fischer, R., et al. (2018). BRAF/MAPK and GSK3 signaling converges to control MITF nuclear export. Proc Natl Acad Sci USA *115*, E8668-8677. 10.1073/pnas.1810498115.
92. Di Malta, C., Siciliano, D., Calcagni, A., Monfregola, J., Punzi, S., Pastore, N., Eastes, A.N., Davis, O., De Cegli, R., Zampelli, A., et al. (2017). Transcriptional activation of RagD GTPase controls mTORC1 and promotes cancer growth. Science *356*, 1188-1192. 10.1126/science.aag2553.
93. Napolitano, G., Di Malta, C., and Ballabio, A. (2022). Non-canonical mTORC1 signaling at the lysosome. Trends in Cell Biol *32*, 920-931. 10.1016/j.tcb.2022.04.012.

94. Acharya, A., and Demetriades, C. (2024). mTORC1 activity licenses its own release from the lysosomal surface. Mol Cell *84*, 4385-4400 e4387. 10.1016/j.molcel.2024.10.008.
95. Zwakenberg, S., Westland, D., van Es, R.M., Rehmann, H., Anink, J., Ciapaite, J., Bosma, M., Stelloo, E., Liv, N., Sobrevals Alcaraz, P., et al. (2024). mTORC1 restricts TFE3 activity by auto-regulating its presence on lysosomes. Mol Cell *84*, 4368-4384 e4366. 10.1016/j.molcel.2024.10.009.
96. Martina, J.A., and Puertollano, R. (2013). RRAG GTPases link nutrient availability to gene expression, autophagy and lysosomal biogenesis. Autophagy *9*.
97. Paquette, M., El-Houjeiri, L., L, C.Z., Puustinen, P., Blanchette, P., Jeong, H., Dejgaard, K., Siegel, P.M., and Pause, A. (2021). AMPK-dependent phosphorylation is required for transcriptional activation of TFEB and TFE3. Autophagy, 1-19. 10.1080/15548627.2021.1898748.
98. Li, S., Song, Y., Quach, C., Guo, H., Jang, G.B., Maazi, H., Zhao, S., Sands, N.A., Liu, Q., In, G.K., et al. (2019). Transcriptional regulation of autophagy-lysosomal function in BRAF-driven melanoma progression and chemoresistance. Nat Commun *10*, 1693. 10.1038/s41467-019-09634-8.
99. Roesch, A., Fukunaga-Kalabis, M., Schmidt, E.C., Zabierowski, S.E., Brafford, P.A., Vultur, A., Basu, D., Gimotty, P., Vogt, T., and Herlyn, M. (2010). A temporarily distinct subpopulation of slow-cycling melanoma cells is required for continuous tumor growth. Cell *141*, 583-594. 10.1016/j.cell.2010.04.020.
100. Roesch, A., Vultur, A., Bogeski, I., Wang, H., Zimmermann, K.M., Speicher, D., Korbel, C., Laschke, M.W., Gimotty, P.A., Philipp, S.E., et al. (2013). Overcoming intrinsic multidrug resistance in melanoma by blocking the mitochondrial respiratory chain of slow-cycling JARID1B(high) cells. Cancer Cell *23*, 811-825. 10.1016/j.ccr.2013.05.003.
101. Chang, J., Campbell-Hanson, K.R., Vanneste, M., Yevdash, J., Bartschat, N.I., Jiang, J.D., Bhinu, A., Helverson, A., Henry, M.D., Steingrimsson, E., et al. (2024). An mTOR-dependent FLCN pathway suppresses TFE3-driven metastasis in melanoma. BioRxiv *doi: https://doi.org/10.1101/2024.07.11.603140*.
102. Aubert, C., Rouge, F., and Galindo, J.R. (1980). Tumorigenicity of human malignant melanocytes in nude mice in relation to their differentiation in vitro. J Natl Cancer Inst *64*, 1029-1040.
103. Zakut, R., Perlis, R., Eliyahu, S., Yarden, Y., Givol, D., Lyman, S.D., and Halaban, R. (1993). KIT ligand (mast cell growth factor) inhibits the growth of KIT- expressing melanoma cells. Oncogene *8*, 2221-2229.
104. Fogh, J., Fogh, J.M., and Orfeo, T. (1977). One hundred and twenty-seven cultured human tumor cell lines producing tumors in nude mice. J Natl Cancer Inst *59*, 221-226.
105. Giard, D.J., Aaronson, S.A., Todaro, G.J., Arnstein, P., Kersey, J.H., Dosik, H., and Parks, W.P. (1973). In vitro cultivation of human tumors: establishment of cell lines derived from a series of solid tumors. J Natl Cancer Inst *51*, 1417-1423.
106. Carey, T.E., Takahashi, T., Resnick, L.A., Oettgen, H.F., and Old, L.J. (1976). Cell surface antigens of human malignant melanoma: mixed hemadsorption assays for humoral immunity to cultured autologous melanoma cells. Proc Natl Acad Sci USA *73*, 3278-3282.
107. Ghanem, G.E., Comunale, G., Libert, A., Vercammen-Grandjean, A., and Lejeune, F.J. (1988). Evidence for alpha-melanocyte-stimulating hormone (alpha-MSH) receptors on human malignant melanoma cells. Int Journal Cancer *41*, 248-255.
108. Herlyn, M., Thurin, J., Balaban, G., Bennicelli, J.L., Herlyn, D., Elder, D.E., Bondi, E., Guerry, D., Nowell, P., Clark, W.H., and et al. (1985). Characteristics of cultured human melanocytes isolated from different stages of tumor progression. Cancer Res *45*, 5670-5676.
109. Herlyn, M., Kath, R., Williams, N., Valyi-Nagy, I., and Rodeck, U. (1990). Growth-regulatory factors for normal, premalignant, and malignant human cells in vitro. Adv Cancer Res *54*, 213-234. 10.1016/s0065-230x(08)60812-x.
110. Westermark, B., Johnsson, A., Paulsson, Y., Betsholtz, C., Heldin, C.H., Herlyn, M., Rodeck, U., and Koprowski, H. (1986). Human melanoma cell lines of primary and metastatic origin express the genes encoding the chains of platelet-derived growth factor (PDGF) and produce

a PDGF-like growth factor. Proc Natl Acad Sci USA *83*, 7197-7200. 10.1073/pnas.83.19.7197.
111. Herlyn, M., Steplewski, Z., Herlyn, D., and Koprowski, H. (1979). Colorectal carcinoma-specific antigen: detection by means of monoclonal antibodies. Proc Natl Acad Sci USA *76*, 1438-1442. 10.1073/pnas.76.3.1438.
112. Cornil, I., Man, S., Fernandez, B., and Kerbel, R.S. (1989). Enhanced tumorigenicity, melanogenesis, and metastases of a human malignant melanoma after subdermal implantation in nude mice. J Natl Cancer Inst *81*, 938-944. 10.1093/jnci/81.12.938.
113. Fogh, J., and Trempe, G. (1975). New human cell lines, 1st Edn Edition (Springer, New York). 10.1007/978-1-4757-1647-4_5
114. Magnúsdóttir, E., Dietmann, S., Murakami, K., Günesdogan, U., Tang, F., Bao, S., Diamanti, E., Lao, K., Gottgens, B., and Azim Surani, M. (2013). A tripartite transcription factor network regulates primordial germ cell specification in mice. Nat Cell Biol *15*, 905-915. 10.1038/ncb2798.
115. Bunk, B., Kucklick, M., Jonas, R., Munch, R., Schobert, M., Jahn, D., and Hiller, K. (2006). MetaQuant: a tool for the automatic quantification of GC/MS-based metabolome data. Bioinformatics *22*, 2962-2965.
116. Martin, M. (2011). Cutadapt Removes Adapter Sequences From High-Throughput Sequencing Reads. EMBnet J. *17*, 10-12 http://dx.doi.org/10.14806/ej.17.1.200.
117. Dobin, A., Davis, C.A., Schlesinger, F., Drenkow, J., Zaleski, C., Jha, S., Batut, P., Chaisson, M., and Gingeras, T.R. (2013). STAR: ultrafast universal RNA-seq aligner. Bioinformatics *29*, 15-21. 10.1093/bioinformatics/bts635.
118. Heinz, S., Benner, C., Spann, N., Bertolino, E., Lin, Y.C., Laslo, P., Cheng, J.X., Murre, C., Singh, H., and Glass, C.K. (2010). Simple combinations of lineage-determining transcription factors prime cis-regulatory elements required for macrophage and B cell identities. Mol Cell *38*, 576-589. 10.1016/j.molcel.2010.05.004.
119. Robinson, M.D., McCarthy, D.J., and Smyth, G.K. (2010). edgeR: a Bioconductor package for differential expression analysis of digital gene expression data. Bioinformatics *26*, 139-140. 10.1093/bioinformatics/btp616.
120. Saldanha, A.J. (2004). Java Treeview--extensible visualization of microarray data. Bioinformatics *20*, 3246-3248. DOI: 10.1093/bioinformatics/bth349.
121. Subramanian, A., Tamayo, P., Mootha, V.K., Mukherjee, S., Ebert, B.L., Gillette, M.A., Paulovich, A., Pomeroy, S.L., Golub, T.R., Lander, E.S., and Mesirov, J.P. (2005). Gene set enrichment analysis: a knowledge-based approach for interpreting genome-wide expression profiles. Proc Natl Acad Sci USA *102*, 15545-15550. 10.1073/pnas.0506580102.
122. Tyanova, S., Temu, T., Sinitcyn, P., Carlson, A., Hein, M.Y., Geiger, T., Mann, M., and Cox, J. (2016). The Perseus computational platform for comprehensive analysis of (prote)omics data. Nat Methods *13*, 731-740. 10.1038/nmeth.3901.
123. Young, L., Sung, J., Stacey, G., and Masters, J.R. (2010). Detection of Mycoplasma in cell cultures. Nat Protoc *5*, 929-934. 10.1038/nprot.2010.43.
124. Louphrasitthiphol, P., Chauhan, J., and Goding, C.R. (2020). ABCB5 is activated by MITF and beta-catenin and is associated with melanoma differentiation. Pigment Cell Melanoma Res *33*, 112-118. 10.1111/pcmr.12830.

Figure 1. Control of mTORC1 regulators by MITF

(A) Western blot of two melanoma cell lines transfected with control or MITF-specific siRNA. ERK and ACTIN are used as loading controls.

(B-C) Heatmaps showing relative mRNA expression of indicated genes in the CCLE melanoma or the Tsoi et al collection of 53 melanoma cell lines.

(D) Plots showing TCGA melanomas ranked by expression of *MITF* (Black line). Expression of *RRAGD* (left) or *FNIP2* (right) in each melanoma is indicated by grey bars and the moving average of each, per 20 melanomas window, is indicated by the colored lines.

(E) UCSC browser screenshots of MITF ChIP-seq showing binding to the *RRAGD* or *FNIP2* genes.

(F) Western blot of melanoma cell lines showing expression of indicated proteins.

(G) Relative expression of indicated genes based on triplicate RNA seq of IGR37 melanoma cells expressing doxycycline-inducible β-catenin (iCTNNB1).

(H) Expression of *RRAGD* and *FNIP2* based on triplicate RNA-seq after shRNA-mediated depletion of MITF in MeWo human melanoma cells.

See also Figure S1.

Figure 2. Differential expression of MITF, TFEB and TFE3 on glucose limitation

(A-C) Plots showing TCGA melanomas ranked by expression of *MITF* (A,B) or TFEB (C) (Black lines). Expression of TFE3 (left and right) or TFEB (middle) in each melanoma is indicated by grey bars, and the moving average of each per 20 melanoma window is indicated by the colored lines.

(D-E) Heatmap showing relative expression of indicated genes in the Tsoi et al panel of melanoma cell lines (D) or an inhouse panel (E).

(F) Western blot of in-house panel of melanoma cell lines for indicated proteins.

(G-H) Western blot showing expression of indicated proteins in 501mel melanoma cells (G) or HT29 colorectal cancer cells (H) following glucose limitation (0.6 mM) for the indicated times.

(I) Flow cytometry of IGR37 cells transfected with control siRNA or a pool of 3 siTFE3 for 48 h before placing cells in glucose-free DMEM for 6 h. Error bars indicate S.D. N=3. *= $p < 0.05$; **= $p < 0.01$; ***= $p < 0.001$; ****= $p < 0.0001$ *ns* = not significant, Student T test.

Figure 3. MITF family members bind a similar repertoire of genes.

(A) Amino acid sequences of the basic region of the MITF family members

(B) Western blot showing expression of doxycycline-inducible HA-tagged TFEB in 501mel cells after treatment with 0, 5 and 25 ng doxycycline.

(C) Jitter plots showing peak scores of HA-TFEB ChIP-seq in 501mel cells treated or not with 250 nM Torin for 6 h and either 0 ng (left) or 5 ng (right) doxycycline. Black lines indicate mean. Boxes indicate interquartile range and median.

(D) Western blot showing expression doxycycline-inducible HA-tagged TFE3 in 501mel cells after treatment with 0, 5 and 25 ng doxycycline.

(E-F) Venn diagrams showing the number statistically significant ChIP peaks for MITF family members with HA-TFEB and HA-TFE3 ChIPs performed in the presence of 250 nM Torin. No doxycycline was used for the HA-TFE3 ChIP and 5 ng for the TFEB ChIP. The MITF data was taken from Louphrasitthiphol et al, 2020.

(G) Plots showing relative peak scores at sites bound by each factor alone or indicted combinations. Boxes indicate interquartile range and median. **** indicates p-value < 0.001 One-way ANOVA.

(H) Motifs identified beneath ChIP peaks for MITF, TFEB and TFE3.

(I) Plot showing genome ontology of the binding sites identified for each factor.

(J) UCSC genome browser screenshots showing color coded ChIP profiles for input control and HA-TFEB, HA-TFE3 and HA-MITF at indicated genes. Only one replicate is shown. Similar results were obtained for replicate 2.

See also Figure S2.

Figure 4. Differential gene expression in *TFEB*, *TFE3* and *TFEB/TFE3* KO human melanoma cells.

(A) Heatmap based on triplicate RNA-seq showing differential gene expression of control 501 mel cells or cells grown in HBSS for 12 h.

(B) Volcano plot showing numbers of significantly (FC ≥ 2, p = <0.05) differentially expressed genes comparing control and HBSS treated cells.

(C) GSEA plots showing significantly differentially enriched gene sets comparing control and HBSS treated 501mel cells.

(D) GSEA plots for the indicated gene sets of control versus HBSS treated 501mel cells.

(E) Western blot using parental and *TFEB* and/or *TFE3* 501mel KO cell lines.

(F-G) Heatmaps based on triplicate RNA-seq showing differential gene expression (FC ≥ 2, p = <0.05) of parental 501mel cells or indicated *TFEB* and/or *TFE3* KO cells.

(H) Volcano plots showing numbers of significantly (FC ≥ 2, p = <0.05) differentially expressed genes comparing parental cells and indicated 501mel KOs.

(I) GSEA plots showing significantly differentially expressed gene sets comparing parental or indicated *TFEB* and/or *TFE3* 501mel KO cells.

See also Figure S3.

Figure 5. TFE3 and TFEB are not equivalent in gene regulation

(A) Western blot with anti-MITF antibody using parental and MITF B16/F10 KO cell line.

(B) Western blot using parental and indicated *MITF*, *TFEB* and *TFE3* B16 KO cell lines.

(C) Heatmaps based on triplicate RNA-seq showing differential gene expression of parental B16 cells or indicated *MITF*, *TFEB* and *TFE3* B16 KO cell lines.

(D-K) GSEA plots showing significantly differentially enriched gene sets comparing parental or indicated *MITF*, *TFEB* and *TFE3* B16 KO cells.

See also Figure S4.

Figure 6. Differential regulation of metabolism and differentiation by MITF, TFEB and TFE3

(A) Seahorse assays measuring extracellular acidification rate (ECAR) (left) and oxygen consumption rate (OCR) right in indicated B16 WT or KO cell lines. Error bars = SD; n=3.

(B) Seahorse assays summarising differential basal OCR between indicated B16 WT or KO cell lines. Error bars =SD; n=3; ns=non significant, *= p<0.05, **= p<0.01, Student t-test comparing to parental WT B16 cells.

(C) ATP production from glycolysis or oxidative phosphorylation by indicated cell lines. Numbers indicate % derived from each source. Error bars =SD; N=3; ns=non significant, *= p<0.05, **= p<0.01, Student t-test comparing to parental WT B16 cells.

(D) Heatmap based on triplicate RNA-seq showing relative expression of indicated genes in parental and B16 *MITF*, *TFEB* and *TFE3* KO cell lines. The genes listed are a subset of those from the HALLMARK Oxidative Phosphorylation gene set.

(E) Heatmap based on triplicate RNA-seq showing relative expression of indicated genes in parental and B16 *MITF*, *TFEB* and *TFE3* KO cell lines.

(F) Heatmap based on triplicate RNA-seq showing relative expression of indicated genes in 501 mel cells in which MITF had been induced using 100 ng doxycycline.

(G) Western blot of 501mel cells expressing ectopic HA-tagged MITF induced with doxycycline for 16 h.

(H-I) Heatmaps based on triplicate RNA-seq showing relative expression of indicated genes in parental and *MITF*, *TFEB* and *TFE3* B16 KO cell lines.

See also Figure S5.

Figure 7. Reduced tumor growth of B16F10 MITF/TFE KO cells *in vivo*

(A) *In vivo* bioluminescent imaging of primary tumors 28 days after subcutaneous injection of luciferase-expressing B16F10 cells (n = 5). Firefly luciferin (120 mg/kg) was injected intraperitoneally. Scale bar of bioluminescent image radiance (photons/sec/cm2/sr) color scale was set to Min = 1.00e5; Max = 1.00e6 for all pictures.

(B) *In vivo* quantification of bioluminescent of primary tumors. Quantification was performed using the automatic ROI tool (n= 5). Graph shows average and standard deviation of radiance. *= $p < 0.05$, **= $p < 0.001$ when compared to WT cells. using a two-tailed Student t-test.

(C) Tumor growth in B16F10-tumor bearing mice. B16F10 cells (WT, *MITF* KO, *TFEB* KO and *TFE3* KO) n = 5 mice/group. Tumor volume was followed using caliper measurement. *= $p < 0.05$, **= $p < 0.001$, *ns* = not significant when compared to WT cells on the last day.

(D) Lung colonization assay imaged 5 weeks after tail vein injection of $2x10^5$ cells from B16F10 WT, *MITF* KO, *TFEB* KO and *TFE3* KO innoculated mice. N=5 per group.

(E) *In vivo* quantification of bioluminescent from lung tumors. Quantification was performed using the automatic ROI tool (n= 5). Graph shows average and standard deviation of radiance. **= $p < 0.001$, *ns* = not significant using a two-tailed Student t-test.

(F) Model showing sequential changes in MITF, TFEB and TFE3 expression following glucose limitation over time.

Supplemental Figure S1. Predominantly nuclear localization of TFEB in melanoma cells

(A) Immunofluorescence in indicated melanoma cell lines treated or not with 250 nM Torin for 1 h using anti-TFEB (green; top panels) or anti-TFE3 (green; bottom panels) and anti-Lamin B (red). Scale bars = 10 μm for 501mel and IGR37, and 20 μm for the IGR39 and WM793 cells for the TFEB panels and 20 μm for the TFE3 panels. Insets for TFEB panels show magnified regions below, and for the control samples an enhanced image is shown to enable to nuclear localization of TFEB to be readily visualized.

(B) Western blot showing fractionated 501mel cell extracts using Lamin B and GAPDH as markers for the nuclear and cytoplasmic fractions. Cells were transfected with control or siMITF for 48 h before treatment with 250 μM Torin or DMSO before fractionation.

(C) Immunohistochemistry on three human melanomas using anti-TFEB antibody (lower panels) and hematoxylin staining (upper panels). Scale bars = 50 μm.

Supplemental Figure S2. ChIP-seq of HA-TFEB and HA-TFE3.

(A) Immunofluorescence using anti HA antibody showing nuclear accumulation of HA-TFEB after treatment with 250 nM Torin for 6 h.

(B) Inter-replicate correlation of ChIP-seq of HA-TFEB performed under indicated conditions. R = Spearman rho.

(C-D) Venn Diagrams showing significant HA-TFEB ChIP-peaks from 501mel cells with or without Torin treatment (C) or in the presence of 5 ng Doxycycline with or without 250 nM Torin (D).

(E) Heatmap of tag density of each HA-TFEB ChIP-seq experiments using 0 or 5 ng doxycycline with or without 250 nM Torin as indicated using ranked MITF ChIP-seq narrow peak as reference genome coordinate and extend +/- 2.5kb.

(F) Immunofluorescence using anti-HA antibody showing nuclear accumulation of HA-TFE3 after treatment with 250 nM Torin for 6 h.

(G) Inter-replicate correlation of ChIP-seq of HA-TFE3 performed under indicated conditions.

(H) Heatmap showing density of each HA-TFE3 ChIP-seq experiments of HA-TFE3 expressed using 0 ng doxycycline with 250 nM Torin using the same ranked MITF narrow peaks reference as in E.

Supplemental Figure S3. Differential regulation of genes in parental or TFEB/TFE3 KO 501mel after Torin treatment.

(A) Heatmaps based on triplicate RNA-seq showing differential gene expression of parental or indicated 501mel *TFEB* and *TFE3* KO cell lines before or after treatment with 250 nM Torin for 12 h.

(B) Volcano plots showing numbers of significantly (FC $\geq$ 2, p = <0.05) differentially expressed genes comparing parental cells and indicated 501mel KOs in the presence or absence of 250 nM Torin for 12 h as indicated.

(C-F) GSEA plots showing significantly differentially enriched gene sets comparing parental or indicated TFEB and TFE3 501mel cells KO cells treated or not with 250 nM Torin for 12 h as indicated.

Supplemental Figure S4. MITF/TFE factors control proliferation.

(A-H) Volcano plots showing numbers of significantly (FC $\geq$ 2, p = <0.05) differentially expressed genes comparing parental cells and indicated B16/F10 KO cells.

(I) CyQuant assays of parental or indicated *MITF*, *TFEB* and *TFE3* B16 KO cells over time after plating of 4000 cells at time =0 h. N=12 (3 biological replicates in quadruplicate). Error bars indicate S.D.

Supplemental Figure S5. MITF factor ChIP at the *MITF*, *TFEB*, *TFE3* and collagen genes.

(A) UCSC genome browser screenshots showing ChIPs of MITF, TFEB and TFE3 at the *MITF* locus.

(B) Heatmap based on triplicate RNA-seq showing relative expression of *MITF*, *TFEB* and *TFE3* in indicated parental and B16 KO cell lines.

(C-E) UCSC genome browser screenshots showing ChIP-seq profiles of HA-TFE3 and HA-TFEB and HA-MITF at the indicated loci. Binding by TFEB to the *TFEB* gene in panel (D) primarily represents an input signal.

(F) Heatmap showing relative gene expression based on triplicate RNA-seq of parental B16 and derived MITF, TFEB and TFE3 KO cells showing genes from the HALMMARK Interferon Alpha Response gene set.

(G) UCSC genome browser screenshots showing ChIP-seq profiles of HA-TFE3 and HA-TFEB and HA-MITF at the CD47 locus.

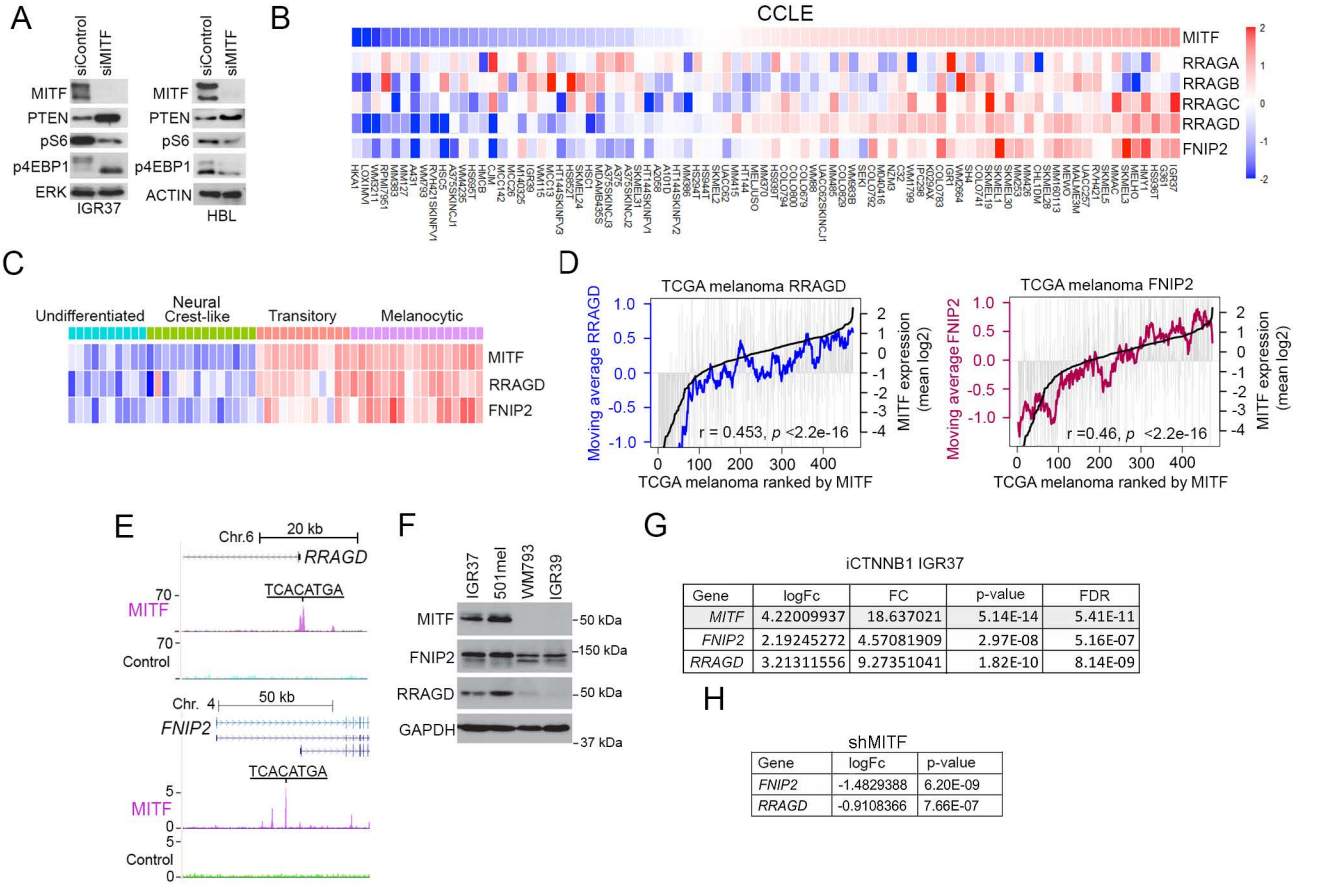

Gene	logFc	FC	p-value	FDR
MITF	4.22009937	18.637021	5.14E-14	5.41E-11
FNIP2	2.19245272	4.57081909	2.97E-08	5.16E-07
RRAGD	3.21311556	9.27351041	1.82E-10	8.14E-09

Gene	logFc	p-value
FNIP2	-1.4829388	6.20E-09
RRAGD	-0.9108366	7.66E-07

Dias et al
FIGURE 1

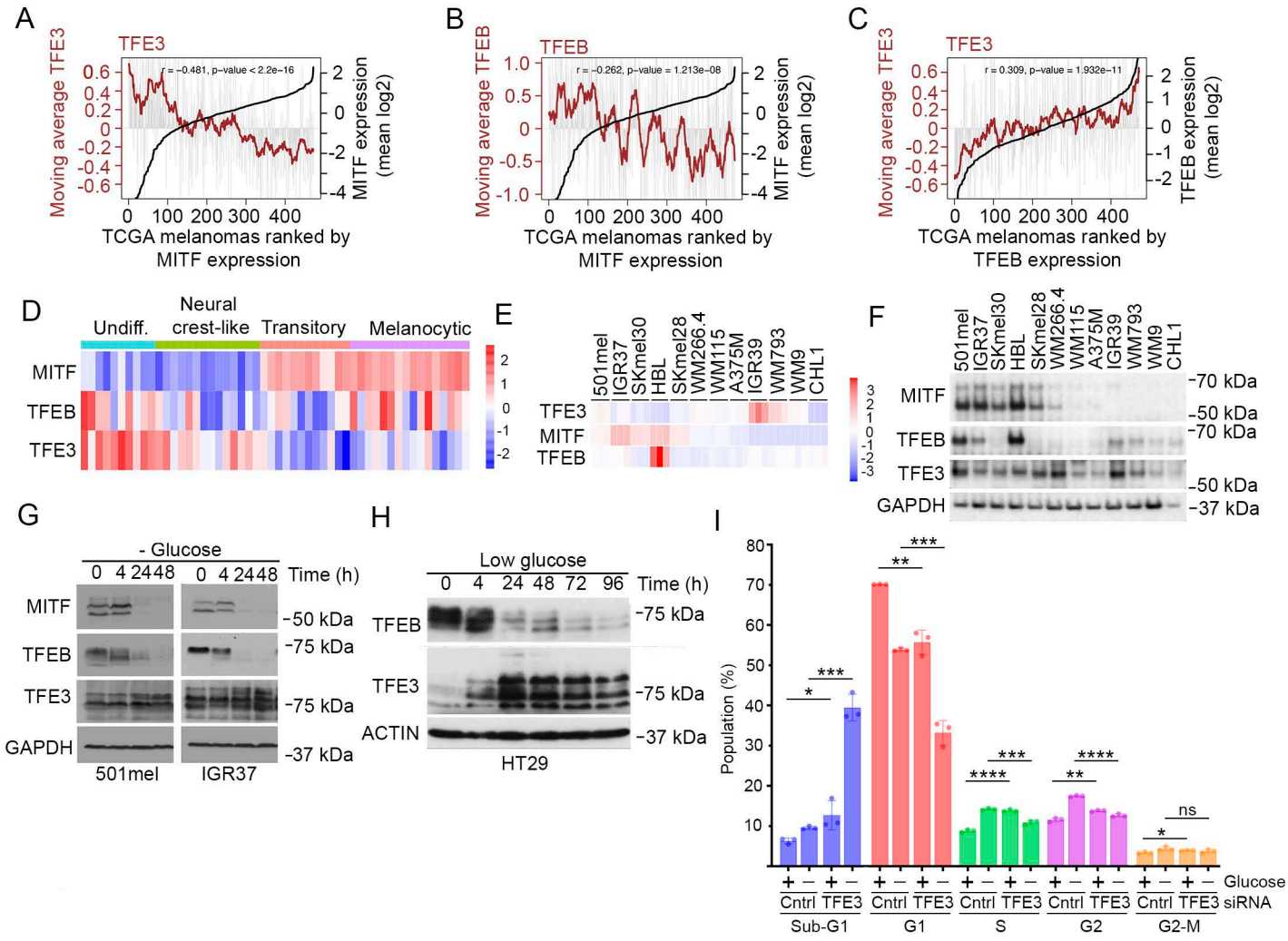

Dias et al
FIGURE 2

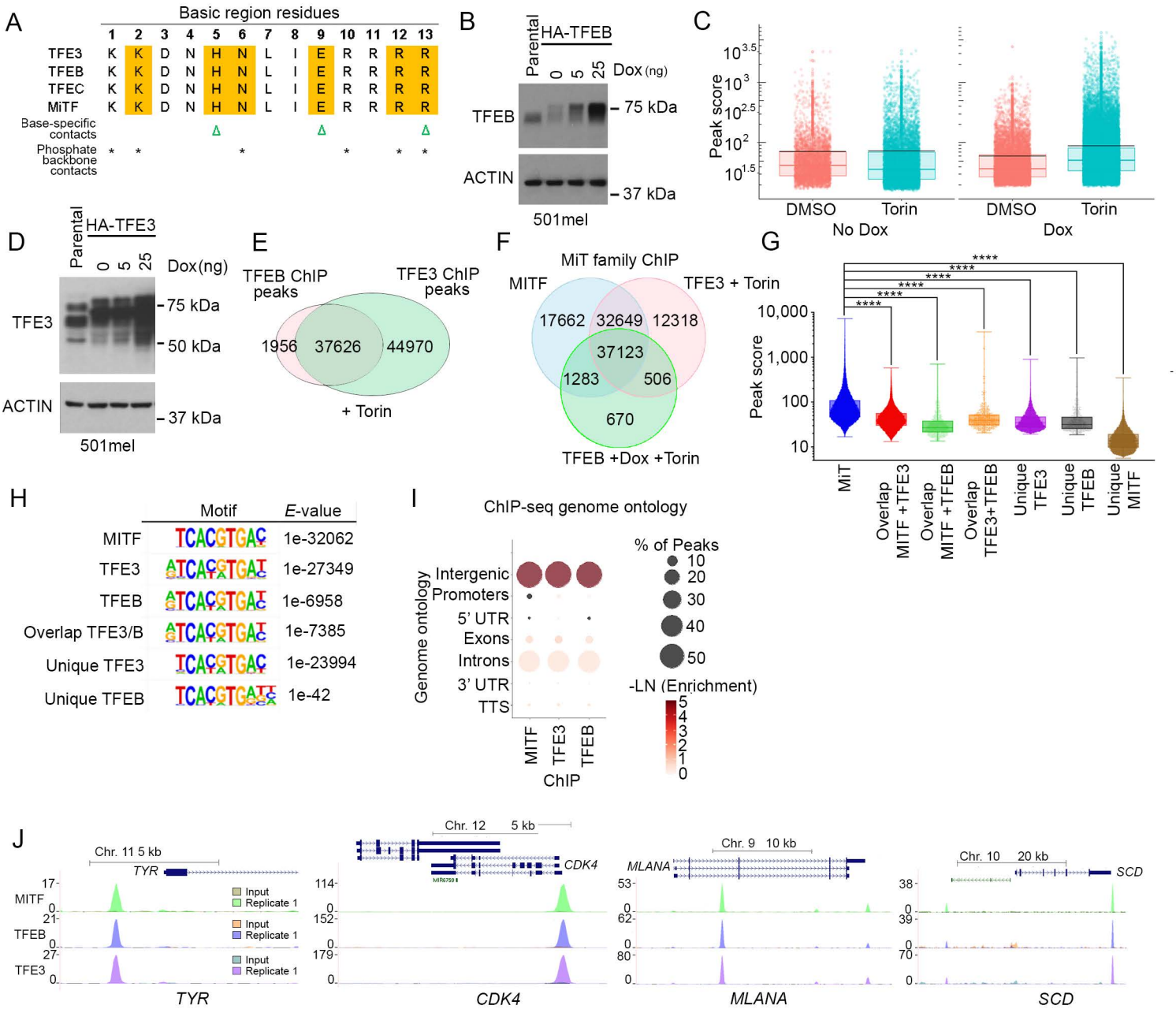

Dias et al
Figure 3

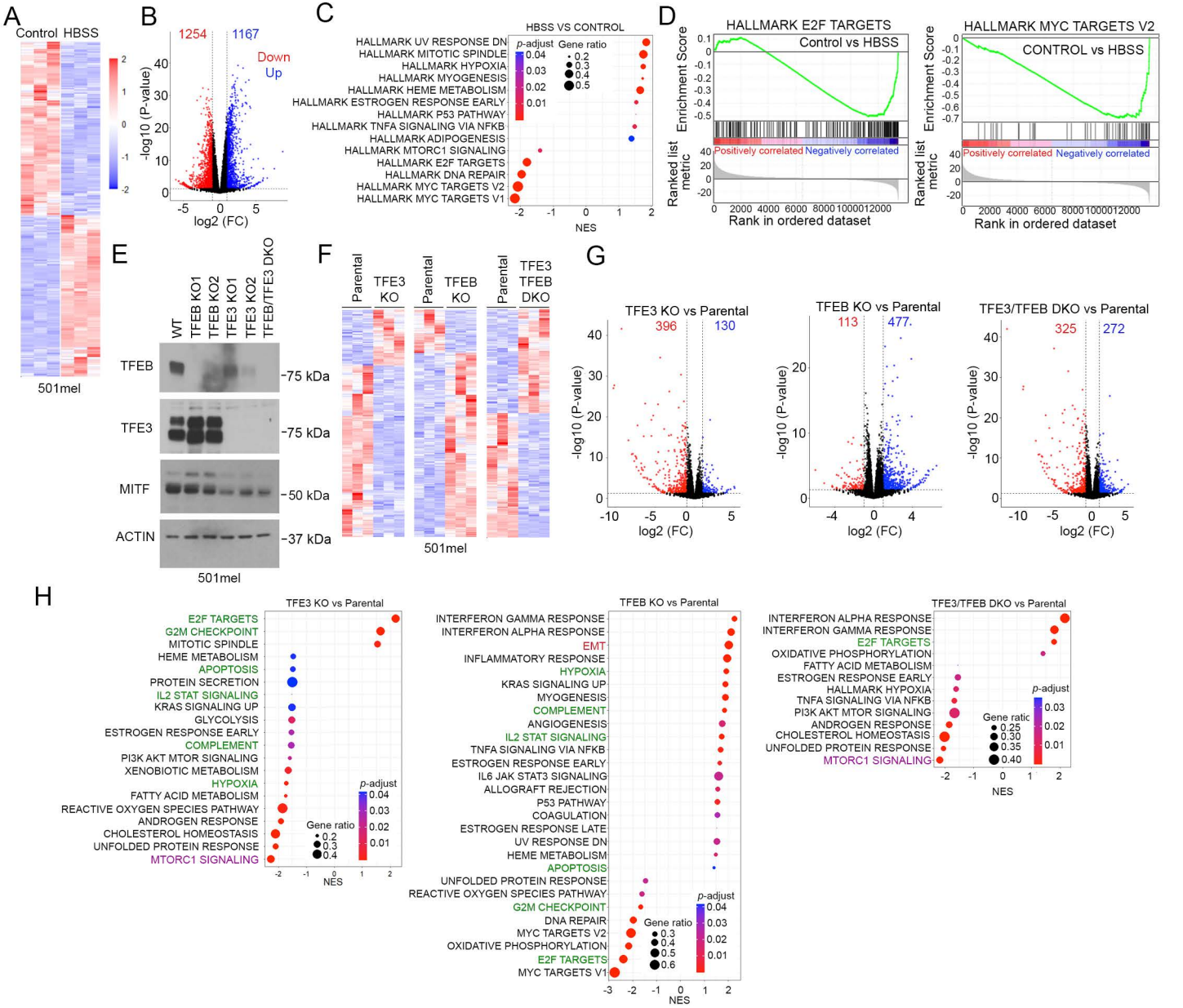

Dias et al
FIGURE 4

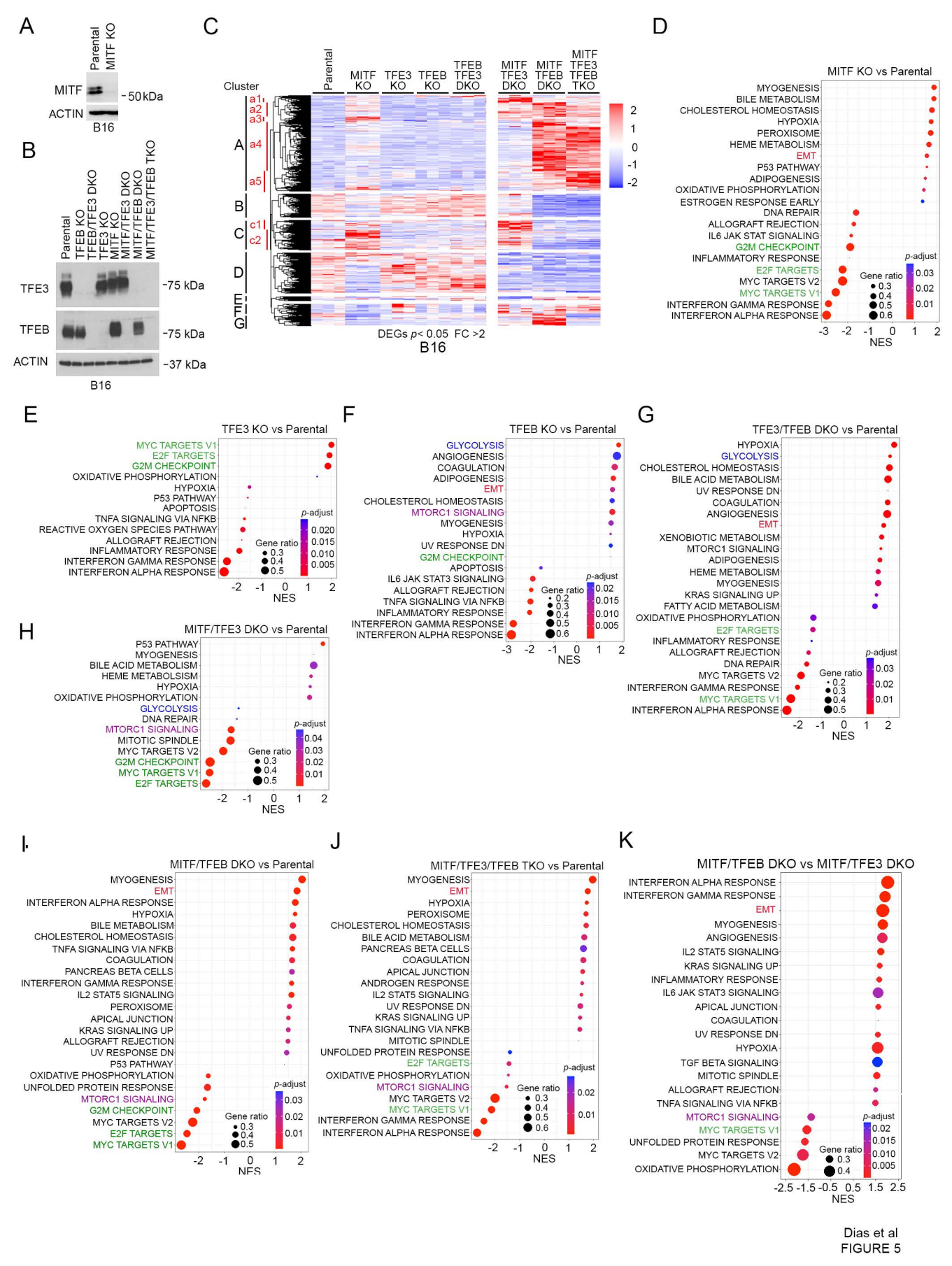

Dias et al
FIGURE 5

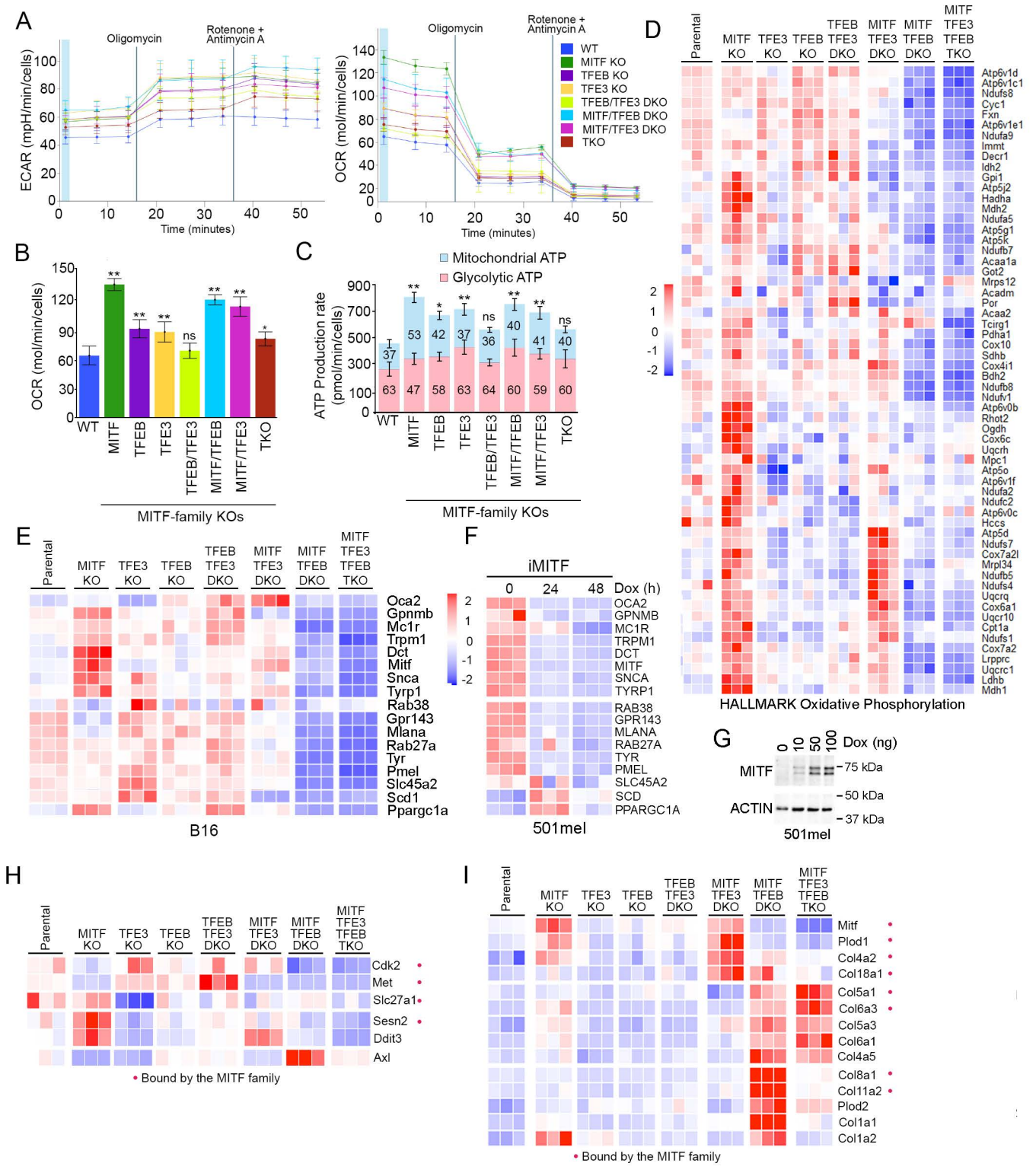

Dias et al
FIGURE 6

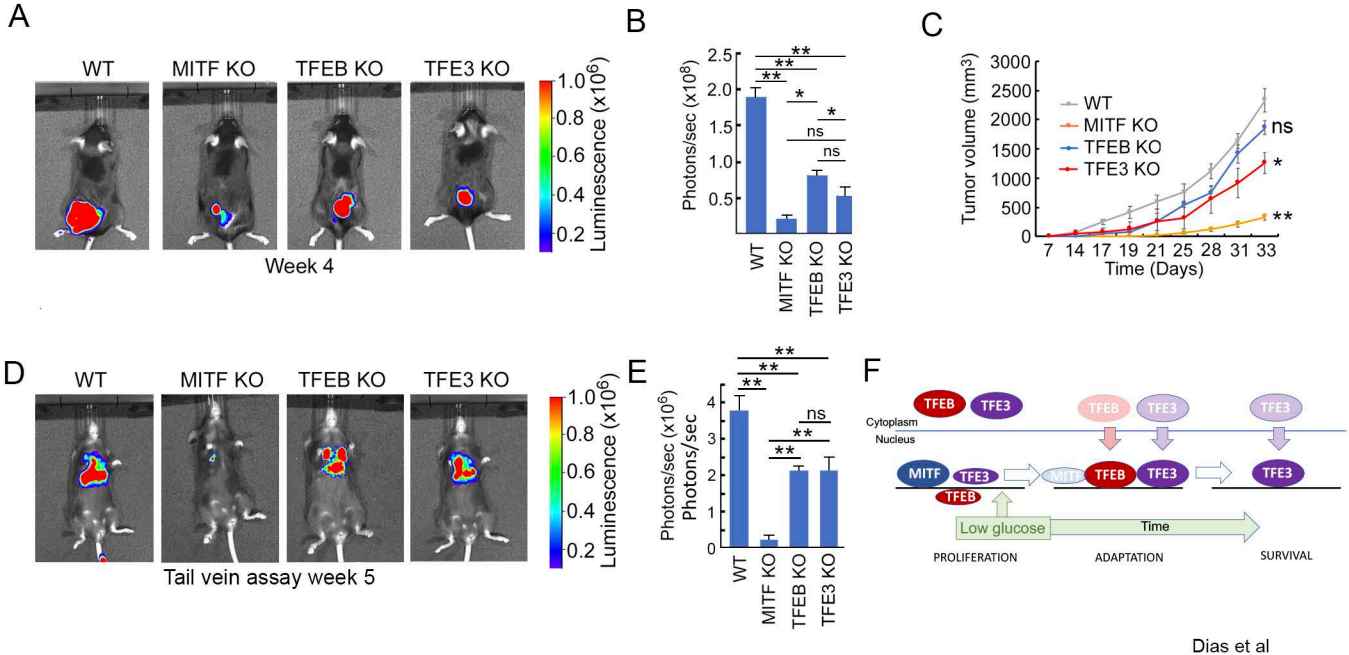

Dias et al
FIGURE 7

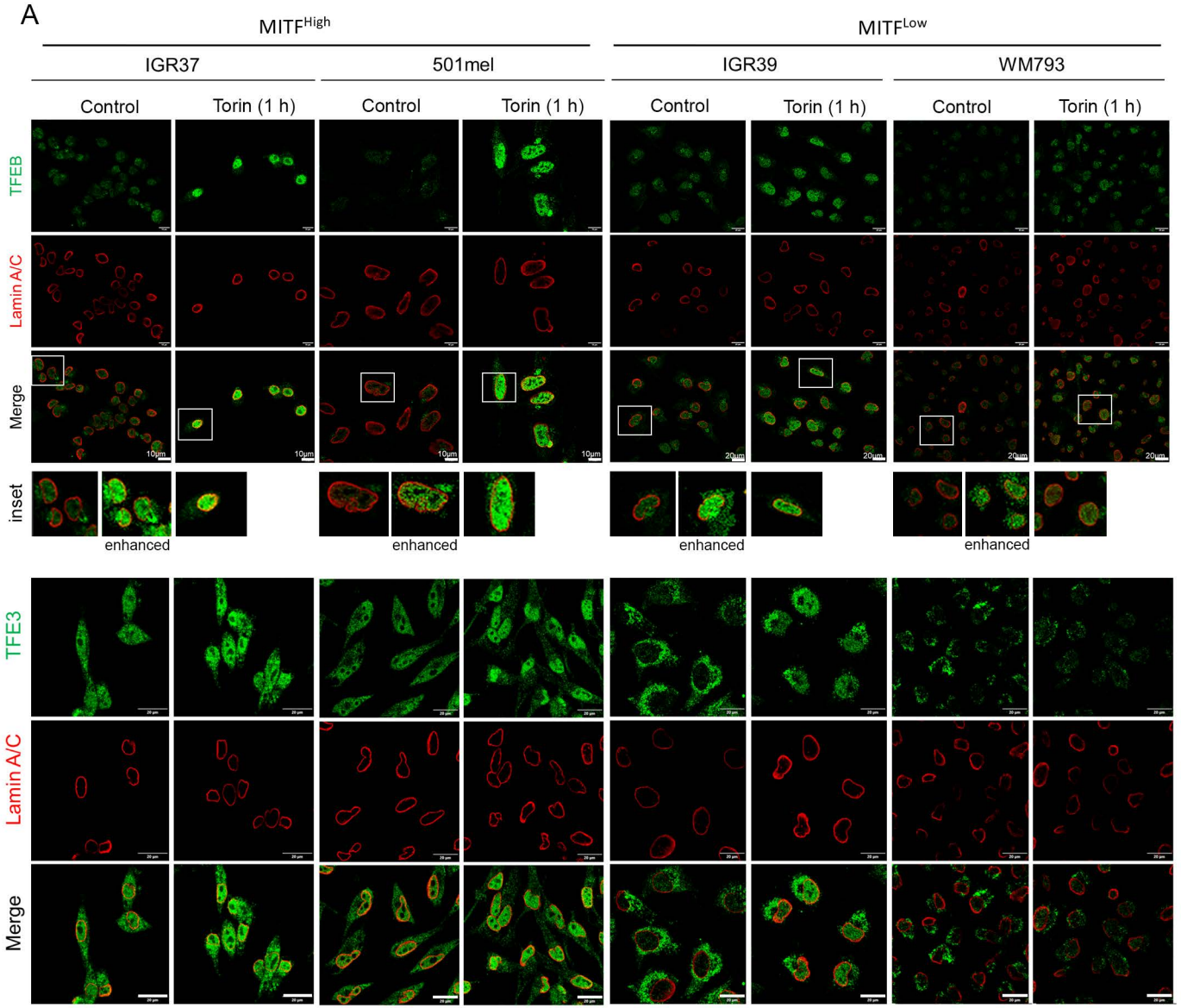

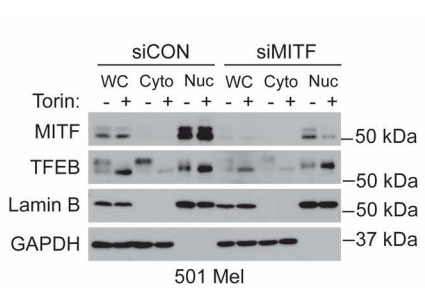

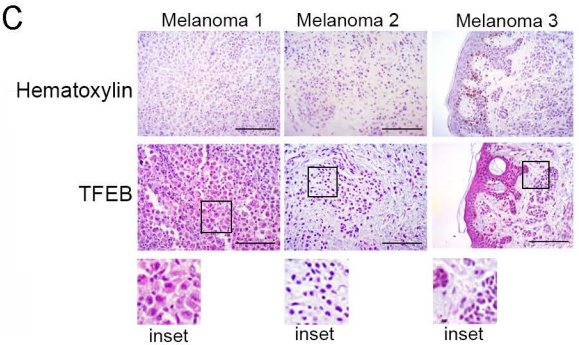

Dias et al
Supplemental Figure S1

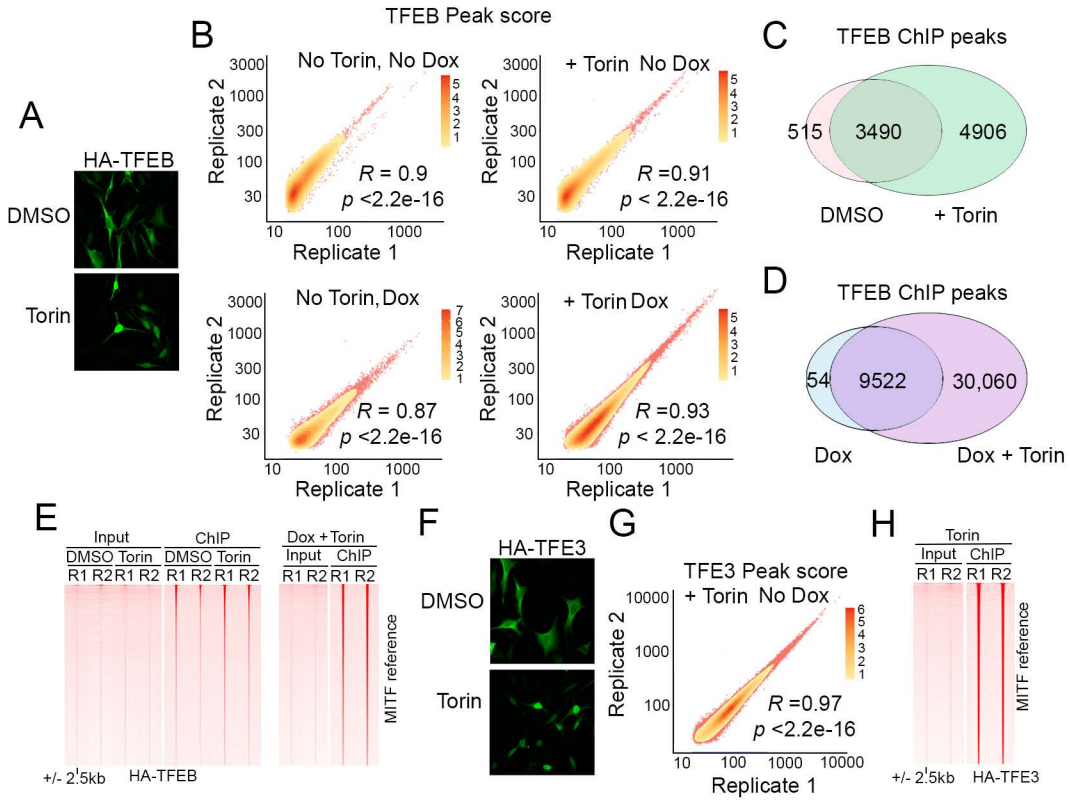

Dias et al
Supplemental Figure S2

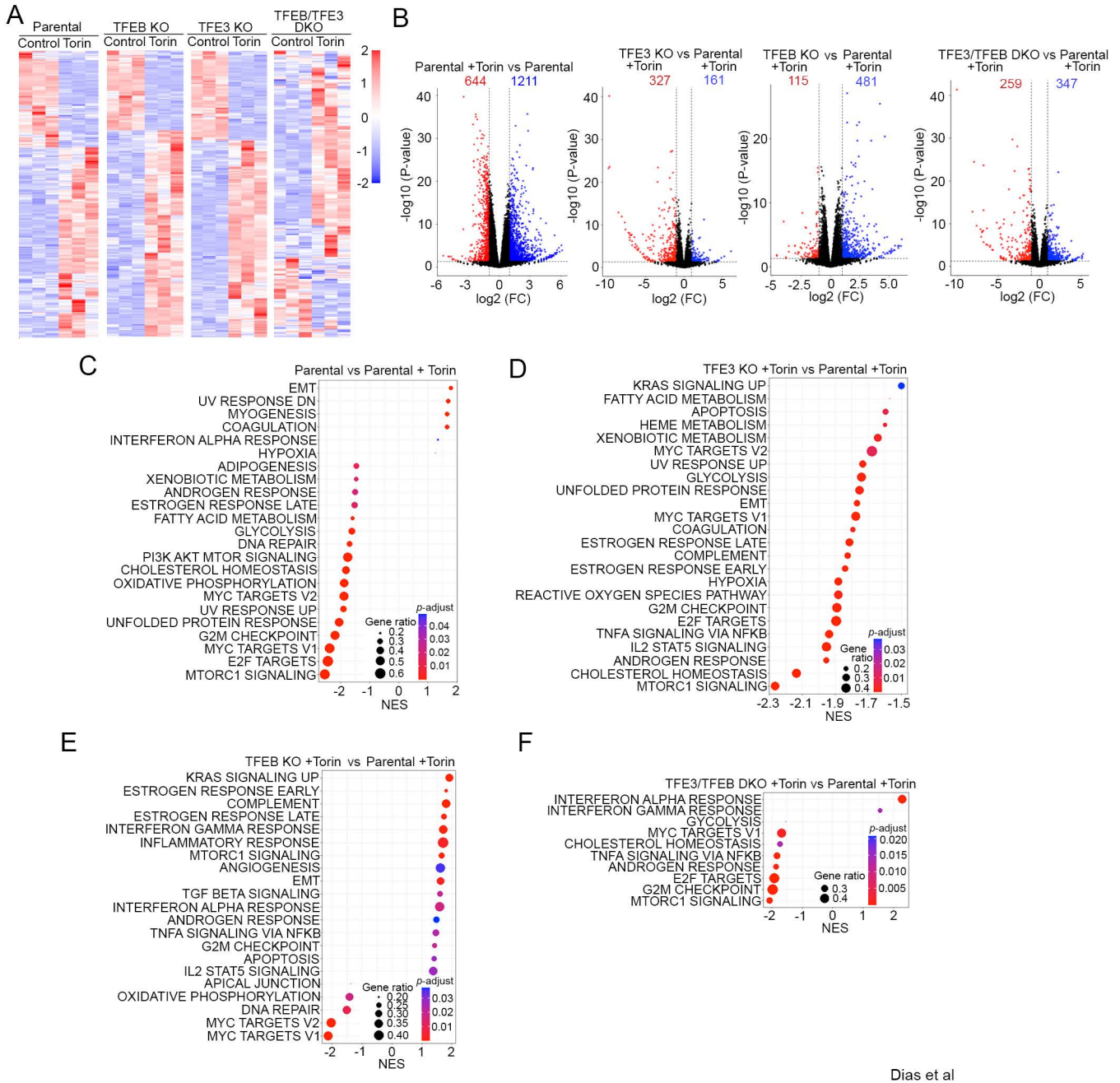

Dias et al
Supplemental Figure S3

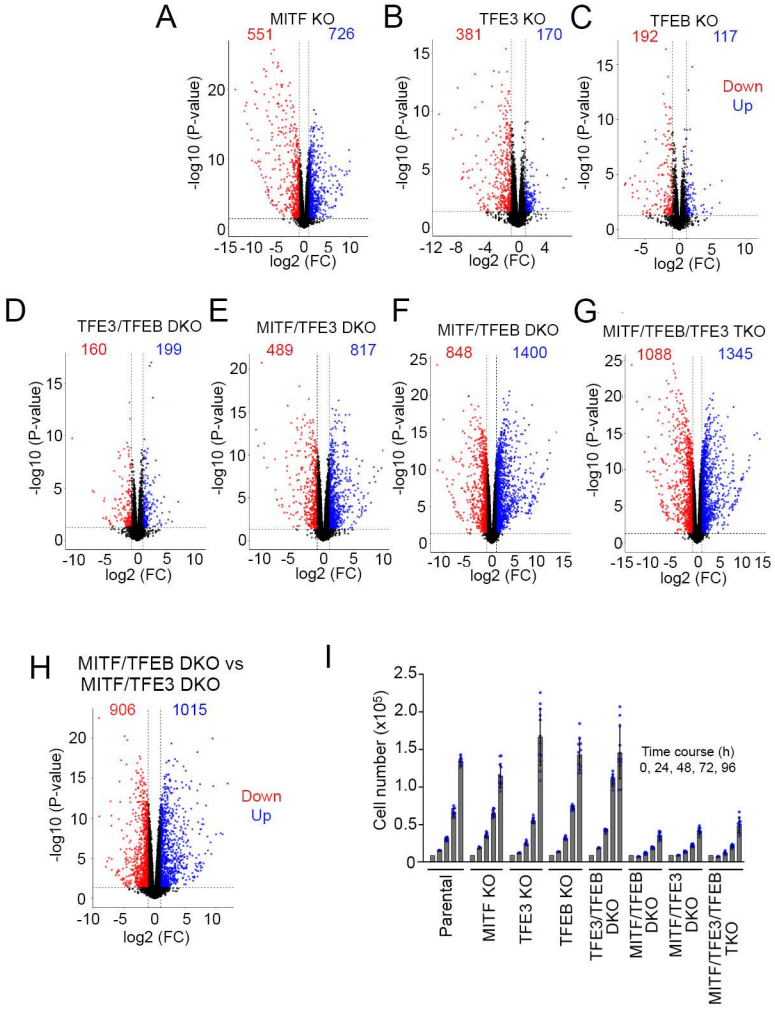

Dias et al
Supplemental Figure S4

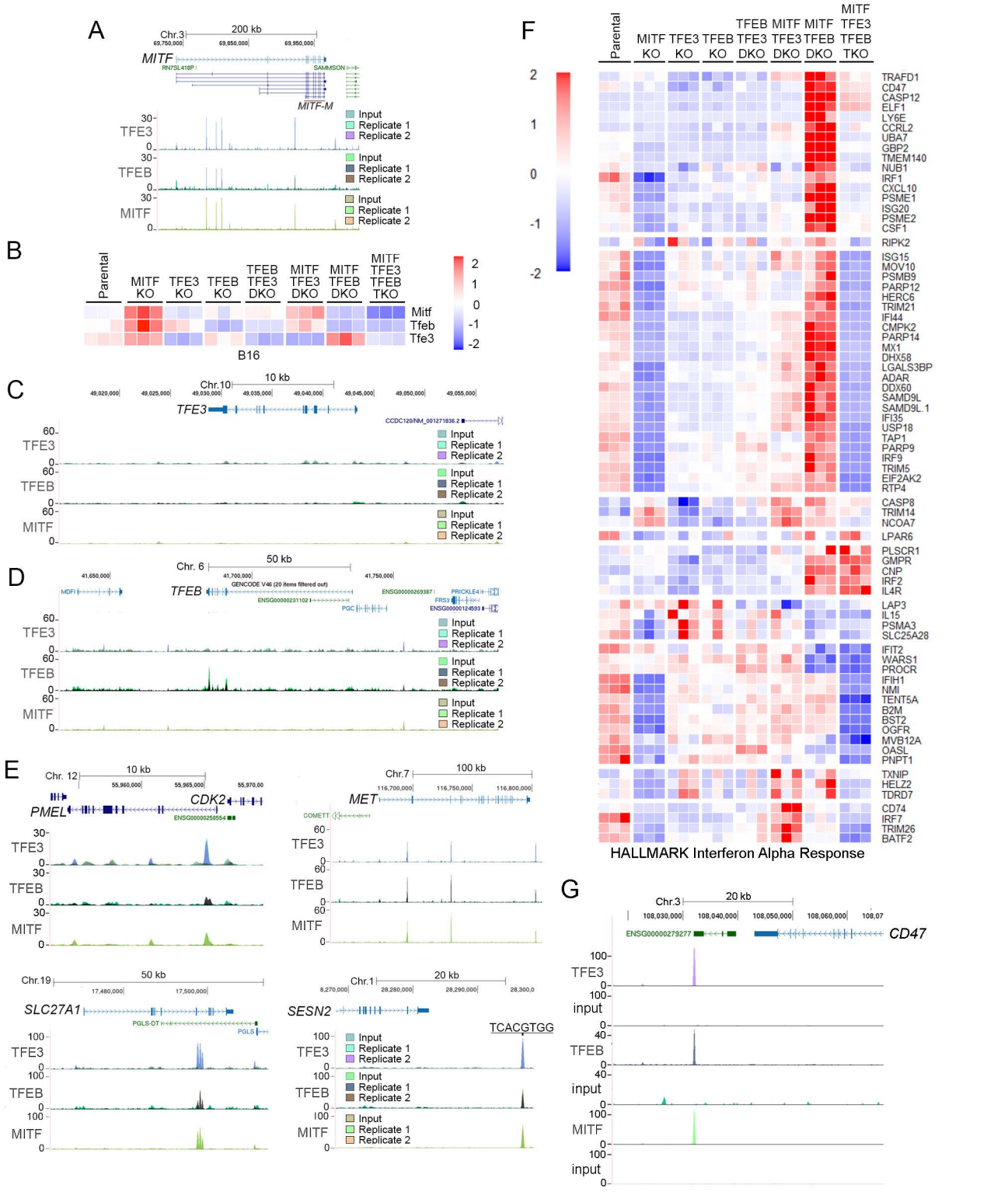

Dias et al
Supplemental Figure S5